Odin/OSIRIS observations of stratospheric BrO: Retrieval methodology, climatology, and inferred Br_y

C. A. McLinden,[1] C. S. Haley,[2] N. D. Lloyd,[3] F. Hendrick,[4] A. Rozanov,[5] B.-M. Sinnhuber,[5] F. Goutail,[6] D. A. Degenstein,[3] E. J. Llewellyn,[3] C. E. Sioris,[1] M. Van Roozendael,[4] J. P. Pommereau,[6] W. Lotz,[5] and J. P. Burrows[5]

Received 15 May 2009; revised 2 February 2010; accepted 16 February 2010; published 11 August 2010.

[1] A 7+ year (2001–2008) data set of stratospheric BrO profiles measured by the Optical Spectrograph and Infra-Red Imager System (OSIRIS) instrument, a UV-visible spectrometer measuring limb-scattered sunlight from the Odin satellite, is presented. Zonal mean radiance spectra are computed for each day and inverted to yield effective daily zonal mean BrO profiles from 16 to 36 km. A detailed description of the retrieval methodology and error analysis is presented. Single-profile precision and effective resolution are found to be about 30% and 3–5 km, respectively, throughout much of the retrieval range. Individual profile and monthly mean comparisons with ground-based, balloon, and satellite instruments are found to agree to about 30%. A BrO climatology is presented, and its morphology and correlation with NO_2 is consistent with our current understanding of bromine chemistry. Monthly mean Br_y maps are derived. Two methods of calculating total Br_y in the stratosphere are used and suggest (21.0 ± 5.0) pptv with a contribution from very short lived substances of (5.0 ± 5.0) pptv, consistent with other recent estimates.

Citation: McLinden, C. A., et al. (2010), Odin/OSIRIS observations of stratospheric BrO: Retrieval methodology, climatology, and inferred Br_y, *J. Geophys. Res.*, *115*, D15308, doi:10.1029/2009JD012488.

1. Introduction

[2] The importance of the inorganic bromine family (Br_y = Br + BrO + HBr + HOBr + $BrONO_2$ + BrCl) has been recognized since the 1970s [*Spencer and Rowland*, 1978] and further elucidated in the 1980s [*McElroy et al.*, 1986]. In the lower stratosphere, catalytic cycles involving bromine are important contributors to ozone destruction, particularly in the midlatitudes. By way of example, one such cycle is

(R1) $$BrO + O \rightarrow Br + O_2$$

(R2) $$Br + O_3 \rightarrow BrO + O_2$$

which results in a net loss of two odd-oxygen ($O+O_3$) molecules. Other cycles involving HOBr and ClO are well-documented [e.g., *Chartrand and McConnell*, 2000] and are not provided here.

[3] Stratospheric Br_y originates from the cross-tropopause transport of bromine-bearing species emitted from the surface. These sources can roughly be classified as (1) methyl bromide (CH_3Br), the single largest source with both natural and anthropogenic components; (2) halons ($CBrClF_2$, $CBrF_3$, $CBrF_2CBrF_2$, and CBr_2F_2), strictly an anthropogenic source; and (3) bromine-bearing very short lived substances (VSLS) such as CH_2Br_2 and $CHBr_3$, with many other possible contributors [*World Meteorological Organization* (*WMO*), 2007]. It is this last source that is the subject of much debate as current estimates of their contribution to the stratospheric budget vary from 1.5 to 8 pptv [*Pfeilsticker et al.*, 2000; *Sinnhuber et al.*, 2005; *Sioris et al.*, 2006; *Kovalenko et al.*, 2007; *Laube et al.*, 2008; *Dorf et al.*, 2008; *Hendrick et al.*, 2008]. The difference between the lower and upper estimate has a large impact on the importance of Br_y on midlatitude ozone depletion [*Salawitch et al.*, 2005].

[4] While profiles of stratospheric HBr were measured from balloon-borne instruments in the 1990s [*Johnson et al.*, 1995; *Nolt et al.*, 1997], BrO is the only member of the Br_y family that has been systematically and globally measured in the stratosphere, a fact that has complicated the closure of the Br_y budget. A very recent exception to this are profiles of $BrONO_2$ observed by the Michelson Interferometer for Passive Atmospheric Sounding (MIPAS) satellite instrument [*Höpfner et al.*, 2009]. In situ measurements of BrO exist

[1]Air Quality Research Division, Environment Canada, Toronto, Ontario, Canada.
[2]Centre for Research in Earth and Space Science, York University, Toronto, Ontario, Canada.
[3]Institute of Space and Atmospheric Studies, University of Saskatchewan, Saskatoon, Saskatchewan, Canada.
[4]Institut d'Aéronomie Spatiale de Belgique, Brussels, Belgium.
[5]Institute of Environmental Physics, University of Bremen, Bremen, Germany.
[6]Service d'Aéronomie, CNRS, Verrières-le-Buisson, France.

0148-0227/10/2009JD012488

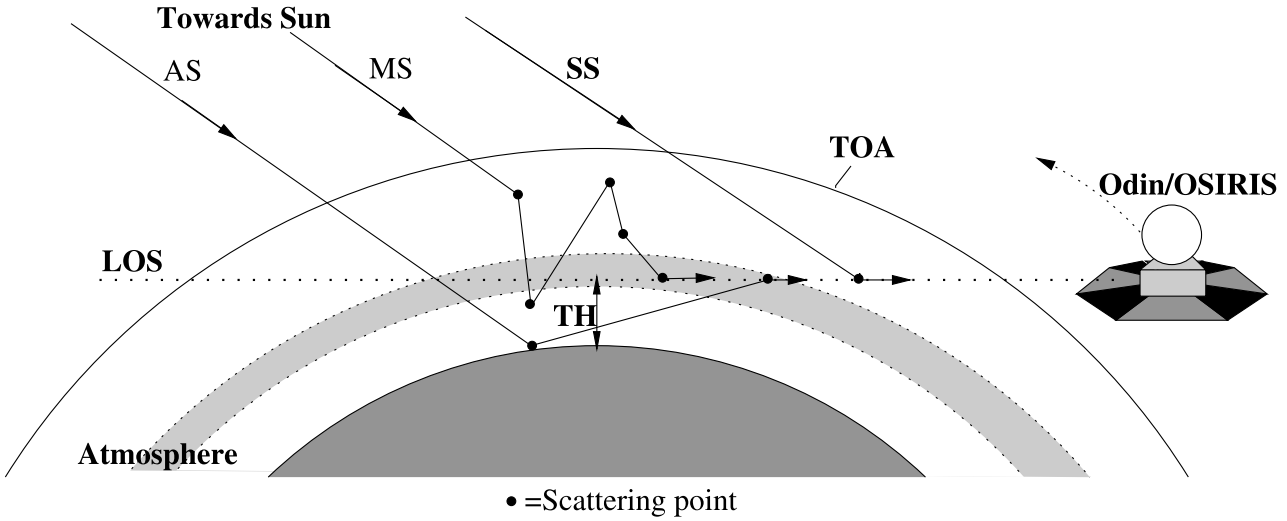

Figure 1. Depiction of the limb-scattering geometry showing examples of single-scattered (SS), multiple-scattered (MS), and surface-scattered (AS) light paths. LOS denotes the OSIRIS line of sight, TH is the tangent height of the LOS, and TOA is top of atmosphere.

[*Brune et al.*, 1988], although these are sparse. Global measurements of the total vertical column density (VCD) of BrO have been made since 1995 by a series of nadir-viewing satellite instruments beginning with Global Ozone Monitoring Experiment (GOME) [*Richter et al.*, 1998]. Ground-based zenith-sky observations of scattered sunlight have been made since the 1980s [*Solomon et al.*, 1989] but, like nadir measurements, yield limited information on the vertical distribution of BrO. Stratospheric BrO profiles from balloon-borne instruments such as Systeme d'Analyse par Observations Zenithales (SAOZ)–BrO [*Pundt et al.*, 2002] and Limb Profile Monitor of the Atmosphere/Differential Optical Absorption Spectroscopy (LPMA/DOAS) [*Dorf et al.*, 2006] have been made semiregularly since the 1990s and for much of the time since remained the only source of profile information. More recently, satellite instruments such as Scanning Imaging Absorption Spectrometer for Atmospheric Chartography (SCIAMACHY) on Envisat [*Bovensmann et al.*, 1999], in limb-scattering mode [*Sinnhuber et al.*, 2005; *Sioris et al.*, 2006; *Hendrick et al.*, 2009], and Microwave Limb Sounder (MLS) on Aura [*Kovalenko et al.*, 2007], have been measuring BrO profiles. However, despite this additional information, the uncertainties in the VSLS contribution to stratospheric Br_y remain. The analysis of the same data are even leading to significant, and as yet unresolved, differences in the VSLS estimate [*WMO*, 2007; A. Rozanov et al., Retrieval of BrO vertical distributions from SCIAMACHY limb measurements, submitted to *Atmospheric Measurement Techniques and Discussions*, 2010].

[5] In this work a new source of stratospheric BrO measurements is introduced, from the Optical Spectrograph and Infra-Red Imager System (OSIRIS) satellite instrument [*Llewellyn et al.*, 2004], which should aid in our understanding and quantification of this important trace gas.

2. OSIRIS on Odin

[6] Odin was launched in February 2001 into a 600 km circular, Sun-synchronous, near-terminator orbit at an inclination of 97.8° and an ascending node at 1800 local solar time (LST) [*Murtagh et al.*, 2002]. From launch until May 2007, Odin was a combination astronomy-aeronomy mission with time divided equally between the two modes. Since then Odin has operated exclusively in aeronomy mode. Odin carries two instruments: the Submillimetre and Millimetre Radiometer (SMR) [*Frisk et al.*, 2003] which measures profiles of N_2O, HNO_3, O_3, and ClO [*Urban et al.*, 2005] and OSIRIS, the focus of this study. The instruments are coaligned and scan the limb of the atmosphere over a tangent height range of 7–70 km in approximately 85 s in a sawtooth pattern during normal stratospheric operations through controlled nodding of the satellite. Over an orbit, Odin makes roughly 65 such limb scans with roughly half in sunlight. Because of Odin's orbit, OSIRIS does not provide profiles in the winter hemisphere, as solar zenith angles exceed 90°.

[7] OSIRIS contains two optically independent components, the Optical Spectrograph (OS) and the Infra-Red Imager (IRI). The IRI is a three-channel camera, imaging the atmospheric airglow emissions near 1.27 μm and 1.53 μm in a limb-viewing tomographic mode [*Degenstein et al.*, 2003]. The OS is a grating spectrometer that measures sunlight scattered from the Earth's limb back into space. The limb-viewing geometry is illustrated in Figure 1. Specifically, OS measures limb-scattered radiance in the spectral range 280 nm to 800 nm at a spectral resolution of ~1 nm (FWHM) at tangent height intervals of roughly 2 km. The detector is a CCD with 1353 × 32 pixels utilized. The width of a single pixel is about 0.4 nm in the spectral dimension, which gives a sampling ratio of 2.5. The instantaneous field of view (FOV) of the OS is 1 km in the vertical and 40 km in the horizontal at the tangent point. When the nodding of the spacecraft and the varying exposure time of the OS (~0.01 s at 10 km increasing to ~2 s at 50 km) are considered, the vertical resolution of the measured limb radiances is found to range from approximately 1 km at 10 km to 2 km at 50 km. For clarity, "OSIRIS" shall be used to reference the Optical Spectrograph.

[8] The OSIRIS scattered sunlight measurements are used to provide vertical profiles of minor stratospheric constituents. Current operational products are O_3 [*von Savigny et al.*, 2003; *Haley and Brohede*, 2007], NO_2 [*Haley et al.*, 2004; *Haley and Brohede*, 2007], and aerosol extinction [*Bourassa et al.*, 2007]. To date, there are roughly 400,000 profiles of each available. Some current research products include an alternative O_3 that extends into the mesosphere [*Degenstein et al.*, 2009], stratospheric OClO [*Krecl et al.*, 2006] and NO_3 [*McLinden and Haley*, 2008], mesospheric OH [*Gattinger et al.*, 2006], and limb polarization [*McLinden et al.*, 2004].

3. Retrieval Methodology and Characterization

[9] This section describes the methods and algorithms used to create the OSIRIS BrO v4.0 data set.

3.1. Creation of Daily Zonal Mean (Level 1) Spectra

[10] A preliminary evaluation of the OSIRIS spectra has revealed that there is generally an insufficient signal-to-noise ratio (SNR) for single-scan inversions of BrO by a factor of roughly 3. This has necessitated the use of co-added spectra, and sufficient SNR can be achieved with the averaging of 10+ spectra. To achieve this, the approach adopted was to create a daily zonal mean Level 1 (L1) product.

[11] Limb scans from each day were collected into averaging bins: 10° wide in latitude and centered at 85°S to 85°N and sorted according to local time: AM (descending half of the orbit) or PM (ascending half of the orbit). The first step in the creation of the daily zonal mean L1 product was quality control (QC). A scan was discarded if (1) there were large (>6 km) gaps in tangent height, (2) it did not span 35 km, (3) Odin was in or near the South Atlantic Anomaly, and/or (4) the Moon was in the field of view. Individual tangent heights or scans were removed if a Level 1 flag or exception was triggered or there was uneven scanning (which could lead to additional noise and/or poor geolocation). Each scan that passed all QC tests was linearly interpolated onto a standard 81 point potential temperature grid spanning 275 to 5800 K, where the potential temperature was obtained from the European Centre for Medium-Range Weather Forecasts (ECMWF) analysis. This range spans the upper troposphere to the middle mesosphere, much larger than the BrO retrieval range (see section 3.2) and was employed to allow the use of this product to as yet unforeseen applications. Given the 1–2 km resolution of OSIRIS, this represents an oversampling of the original radiances. Other interpolation methods, e.g., cubic spline, have been investigated, and the difference was found to be minimal. The interpolated scans were then averaged for each bin to create daily zonal mean spectra. As Odin resides in a Sun-synchronous orbit, all scans within an averaging bin are measured at virtually the same LST or solar zenith angle (SZA).

[12] Once the mean spectra were calculated, they were then linearly interpolated back onto a standard 6–70 km altitude grid in 2 km increments. This was accomplished by simultaneously calculating the mean altitude associated with each standard potential temperature level. Because of Odin's orbit, not every bin is populated in a given day, and when the entire day is spent in astronomy mode, there is no data at all. When data are available, typically 10–25 scans are averaged, giving an increase in SNR of roughly a factor of 3–5. Since Odin went into aeronomy mode full time in May 2007, the number of scans in a bin is consistently 20–25.

[13] The calculated zonal mean spectra have been inverted to yield daily zonal mean NO_2 to determine what, if any, difference there might be between it and the operational NO_2 [*Haley et al.*, 2004; *Haley and Brohede*, 2007], inverted from individual limb scans, and then averaged over a day. This was done for several days throughout the mission, and differences were found to be small, never exceeding 1%. This suggests that the BrO obtained from daily averaged spectra would be representative of the daily mean of BrO profiles obtained from individual scans.

3.2. Spectral Analysis

[14] The BrO retrieval method is adapted from the OSIRIS NO_2 algorithm [*Haley et al.*, 2004; *Haley and Brohede*, 2007] and is similar to that used for the retrieval of OClO from OSIRIS [*Krecl et al.*, 2006]. Stratospheric profiles of BrO were retrieved in two steps, with the first being a spectral fit [*Haley et al.*, 2004] to obtain so-called apparent slant column densities (SCDs), which represent the absorber-weighted path length through the atmosphere. The second step was an inversion of these SCDs into number density profiles using optimal estimation [*Rodgers*, 2000], described in section 3.5.

[15] Tangent heights of 16–36 km were used in the inversion. Each daily zonal mean OSIRIS radiance spectrum in this altitude range is divided by a reference spectrum in order to remove Fraunhofer structure. The reference spectrum adopted is the mean over all tangent heights from 38–46 km from the same zonal L1 scan. A spectral fit to the logarithm of this radiance ratio was performed between 346.0–376.6 nm, which contains five BrO absorption features (the 5,0 to 1,0 bands) spanning 79 OSIRIS pixels. The basis functions used in the fit include BrO cross sections at 228 K [*Wilmouth et al.*, 1999], ozone at 203, 223, and 243 K [*Bogumil et al.*, 2003], NO_2 at 220 K [*Vandaele et al.*, 1998], and O_4 (Belgian Institute for Space Aeronomy, http://www.aeronomie.be/spectrolab/o2.htm). In addition, a tilt/undersampling pseudo-absorber [*Sioris et al.*, 2003; *Haley et al.*, 2004] and a third-order closure polynomial were included. Sensitivity studies were conducted and found that including a correction for the Ring effect [*Sioris et al.*, 2002] and polarization features [*McLinden et al.*, 2002b] were unnecessary and so were excluded. All cross sections have been corrected for the so-called I_0 effect [*Aliwell et al.*, 2002; *Haley et al.*, 2004]. Also, a relative wavelength shift between the OSIRIS radiances and the basis functions is calculated and then applied [*Haley et al.*, 2004].

[16] An example of a representative spectral fit is shown in Figure 2. In this example, 20 individual scans were averaged over, and the root-mean-square (RMS) residual (over wavelength) is 6.7×10^{-4}. To highlight the BrO absorption features, the fitted closure polynomial was removed from this spectrum. Upon averaging over a large number of residual (the difference between the fitted and measured) spectra, a common feature, or mode, emerged. The RMS of this common mode was about 3×10^{-4}. To assess what impact it had on the fitted BrO amount, it was used as an additional basis function in the spectral fit. Its impact was

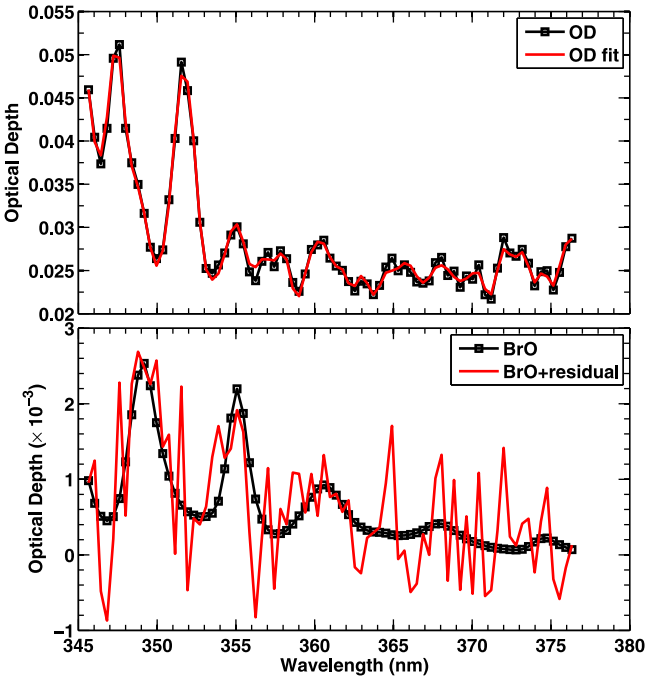

Figure 2. Sample spectral fit for BrO from 15 March 2003, latitude of 55°N, AM, tangent height of 22 km (descending node; 0651 LST; SZA = 85.8°). (top) The fit to the measured OSIRIS differential optical depth (OD) spectrum. (bottom) The fitted BrO. The RMS residual (over wave length) is 6.7×10^{-4}, and the analyzed spectrum is the mean over 20 individual measurements. Each square denotes an OSIRIS pixel. To highlight the absorption features, the fitted closure polynomial has been subtracted.

found to be small, less than 3%, and appeared to be random. On this basis, it was concluded that inclusion of the mean residual in the spectral fit was not necessary, and not a significant source of error. An example of a SCD profile from 15 March 2003 at 55°N and its fitting uncertainty and RMS residual profile is shown in Figure 3.

3.3. Photochemical Box Model

[17] In this work the University of California, Irvine, photochemical box model [*Prather*, 1992; *McLinden et al.*, 2000; *Brohede et al.*, 2008] was employed to (1) calculate BrO a priori profiles required by the inversion (see section 3.5), (2) map the retrieved OSIRIS profiles from their local time to that of another measurement to facilitate a comparison, and (3) derive an estimate of total Br_y. In all applications, ozone, the NO_y, Cl_y and Br_y families, and long-lived species (N_2O, CH_4, and H_2O) were fixed. The remaining species were calculated to be in a 24 h steady state by integrating the model for 30 days with the diurnal cycle fixed on a specified Julian day. Photochemical rate data from the JPL 2006 compendium [*Sander et al.*, 2006] were used.

[18] For the calculation of the a priori BrO, a set of tables were precomputed 3 times per month (for the 1st, 11th, and 21st day), every 2.5° in latitude, and at pressure altitudes between $z^* = 8$ and 56 km in 2 km steps (where $z^* = -16\log(p/1000)$ and p is pressure in hPa) with the entire diurnal cycle of BrO archived. The Br_y abundance in the model was specified using the "organic" N_2O-Br_y correlation [*Wamsley et al.*, 1998; *Salawitch et al.*, 2005], adjusted to 2005 levels of N_2O, with an additional 4 pptv to account for VSLS not included in the *Wamsley et al.* [1998] correlation, thus giving a total Br_y of about 20 pptv. Monthly mean climatologies for temperature [*Nagatani and Rosenfield*, 1993] and ozone [*McPeters et al.*, 2007] were used. The remaining species were either from three-dimensional model output (N_2O, NO_y) [*Olsen et al.*, 2001] or tracer correlations (H_2O,

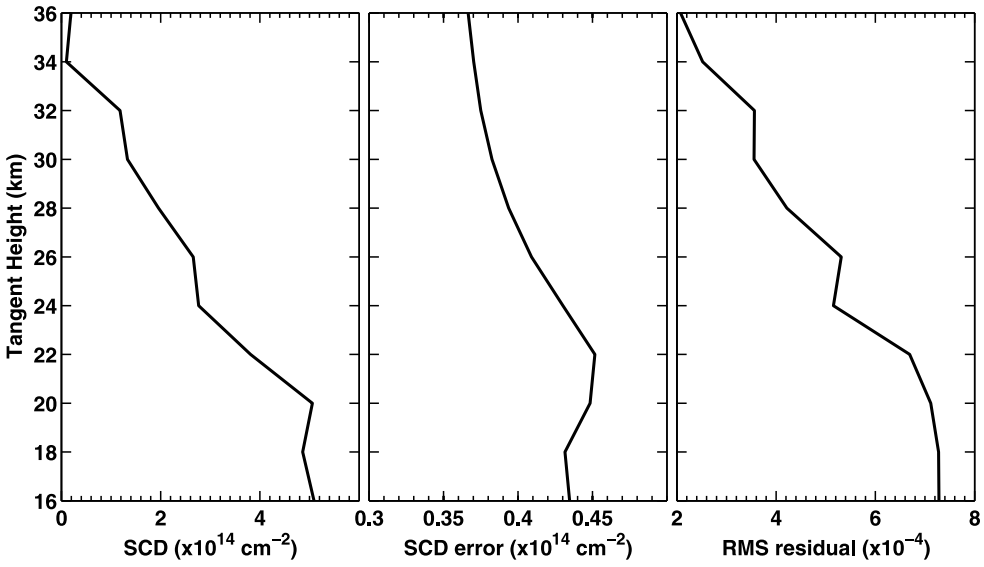

Figure 3. Sample BrO slant column density (SCD) profile, the SCD uncertainty profile (standard error of the SCD) as determined from the spectral fit, and the RMS (over wave length) fitting residual from 15 March 2003, latitude of 55°N, AM (descending node; 0651 LST; SZA = 85.8°).

Cl_y). Linear interpolation in SZA from the tables (using the nearest latitude and Julian day) to the SZA of the measurement (zonal Level 1 profile) was performed.

[19] For intercomparisons of BrO profiles, simulations were constrained using Odin observations in order to better capture the diurnal cycle. These constraints included OSIRIS ozone [*Degenstein et al.*, 2009], SMR monthly mean N_2O [*Urban et al.*, 2005], and Odin-NO_y [*Brohede et al.*, 2008]. Pressure and temperature were taken from the ECMWF analysis. The latitude and the Julian day were set according to the comparison specifics. All remaining settings remained the same as used to generate the tables.

[20] In the determination of Br_y, the monthly mean fields were again used in the calculation of the BrO/Br_y ratio required to convert BrO to Br_y. Results from an investigation into the ability of the box model to simulate NO_y partitioning through comparisons with the JPL MkIV interferometer measurements indicated good agreement [*Brohede et al.*, 2008].

3.4. Radiative Transfer

[21] A radiative transfer (RT) model capable of accurately simulating multiple scattering in limb geometry is required for any inversion of limb-scattered spectra. In this work the LIMBTRAN model [*Griffioen and Oikarinen*, 2000] was employed. For the simulation of a given OSIRIS scan, LIMBTRAN was initialized with a zonal mean temperature and neutral density profile from ECMWF analysis fields and ozone from a zonal mean climatology [*McPeters et al.*, 2007]. In addition, a stratospheric aerosol extinction climatology [*Bauman et al.*, 2003] was employed assuming a Henyey-Greenstein phase function with an asymmetry parameter of 0.7, following *Haley et al.* [2004]. LIMBTRAN accounts for variations in SZA and the change in azimuthal angle (dAZ) along the tangent pathline of sight (LOS). When the change in SZA at the tangent point over the course of a scan becomes important, multiple LIMBTRAN runs were used to account for this. Simulated radiances were calculated on a 1 km vertical grid and at 1 nm increments (in contrast to NO_2 in which radiances were calculated every 2 nm). To reduce the CPU burden, weighting functions were calculated numerically at two wavelengths (355, 365.5 nm), in single-scattering, and assuming no aerosols.

[22] While LIMBTRAN accounts for the variation of SZA along the LOS, it does not allow for any photochemical variability along the LOS. BrO experiences a large change through sunrise and sunset as a result of photochemistry and this may lead to a source of systematic error in the retrieval: the so-called diurnal effect [*McLinden et al.*, 2006]. A research version of the retrieval algorithm using the Vector Orders-of-Scattering Radiative Transfer (VECTOR) model [*McLinden et al.*, 2002a, 2006] does account for this, but the additional CPU requirements make this impractical for operational retrievals. As a result, only limb scans measured at a SZA of 87° or smaller were considered.

3.5. Inversion

[23] The second step in the retrieval is the conversion of BrO SCDs derived from the spectral fit to number density profiles. This is an inverse problem, which uses the RT model, the measured quantities, and some a priori information. The LIMBTRAN forward model, consisting of the results of applying a spectral fit to RT model simulated radiances, was used to map the state-space (BrO profile) into the measurement space (the SCDs). In this study, the retrieval grid was chosen to be a 2 km altitude grid from 16 km to 36 km.

[24] The inversion was accomplished using optimal estimation, or more specifically, the maximum a posteriori (MAP) estimator from *Rodgers* [2000], solved in a Gauss-Newton iterative way [*Haley et al.*, 2004]. MAP is a Bayesian estimator giving the most probable solution based on the measurements and a priori information and the associated covariances. The a priori BrO was taken from the pre-calculated tables (section 3.3). An uncertainty of 100% was assigned to this. The off-diagonal elements in the a priori covariance matrix were constructed using a Gaussian correlation function with a constant correlation length (FWHM) of 4 km. This acts as a smoothing constraint to reduce measurement noise. It is noted that the 100% uncertainty and 4 km correlation length are ad hoc values and not in any way based on a measurement ensemble.

[25] LIMBTRAN was then used to calculate synthetic limb radiances and weighting functions. The weighting functions, calculated using successive perturbations, describe how the forward model responds to a change in the BrO profile [*Haley et al.*, 2004]. On the basis of these calculations, the observations, their uncertainties, and a priori information, MAP then determined an updated BrO profile which was used in LIMBTRAN for the next iteration. To avoid negative densities, a positive constraint was applied to the retrievals by inverting the natural logarithm of BrO number density. A discussion on how the transformation into logarithm-space affects retrievals and statistics is provided by *Brohede et al.* [2007b] in the context of OSIRIS NO_2. In this case, no significant bias was found, and the shape of distribution was minimally affected. Similar conclusions are expected for BrO. Results from a sample measurement from 15 March 2004 (AM) at 45°N are shown in Figure 4.

3.6. Retrieval Characterization and Error Analysis

[26] The MAP approach provides diagnostics that are very useful in characterizing the inverted profiles, including the averaging kernels, measurement response, and resolution. Examples of these are shown in Figure 4. The resolution, or the effective resolution of the inverted profile, was quantified as the full width at half maximum (FWHM) of the averaging kernels. The measurement response is given by the area of the averaging kernels and indicates the relative contribution of the measurements and a priori information to the retrieved profile. A value of 1 implies that the retrieved profile is based solely on the measurements, whereas a value of 0 indicates that the measurements had no contribution to the retrieved profile. Another important diagnostic is the information content of the measurements, which can be quantified by the degrees of freedom for signal, or DOFS [*Rodgers*, 2000], by calculating the trace of the averaging kernel. The DOFS may be interpreted as the number of independent pieces of profile information. This example has a DOFS of 5, and values are generally in the range of 4–6. Characteristics of the data set are shown in Figure 5.

[27] As described by *Rodgers* [2000], four different sources of error can be identified: (1) smoothing error, (2) retrieval

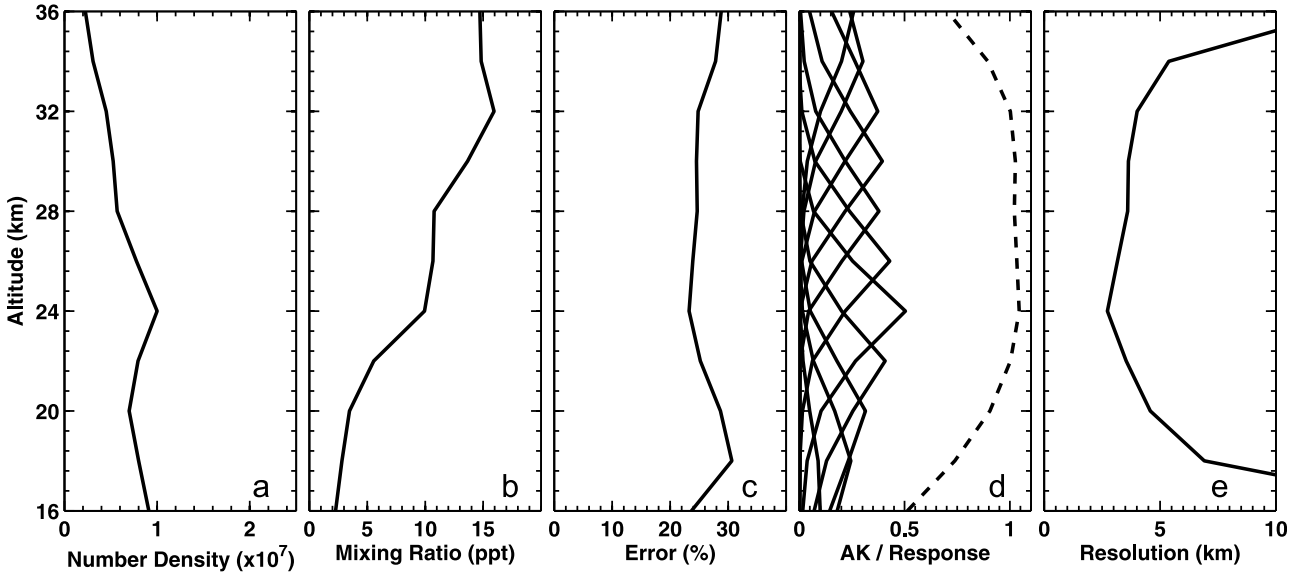

Figure 4. BrO retrieval and diagnostics from 15 March 2003, latitude of 55°N, AM (descending node; 0651 LST; SZA = 85.8°): (a) number density (cm^{-3}); (b) volume mixing ratio (VMR); (c) relative retrieval error; (d) averaging kernels (AK) (solid) and retrieval response (dashed); and (e) retrieval resolution. The degrees of freedom for signal, a measure of the number of independent pieces of information, is 5 in this example.

noise, (3) forward model error, and (4) forward model parameter error.

[28] The forward model error arises from an imperfect description of the physics in the RT model as well as approximations made in order to reduce the CPU requirements. Forward model parameter error is due an imperfect knowledge of the parameters that impact the modeled limb radiances, including the aerosol, temperature, ozone, and neutral density profiles, surface albedo, and absorption cross sections.

[29] Quantifying the forward model and forward model parameter errors requires an off-line sensitivity analysis using noise-free synthetic measurements. For this a midlatitude atmosphere with a SZA of 85°, a change in azimuthal angle of 90°, and a surface albedo of 0.3 were specified. This follows the procedure used by *Haley et al.* [2004]. The forward model error was assessed by simulating spectra using more stringent model settings and then performing a retrieval using the standard settings. Aspects examined were vertical resolution, the use of convolved cross sections (as opposed to convolution of simulated high-resolution spectra), neglecting polarization, and the number of different SZAs simulated along the LOS. The total forward model error was determined by adding together the individual components. It

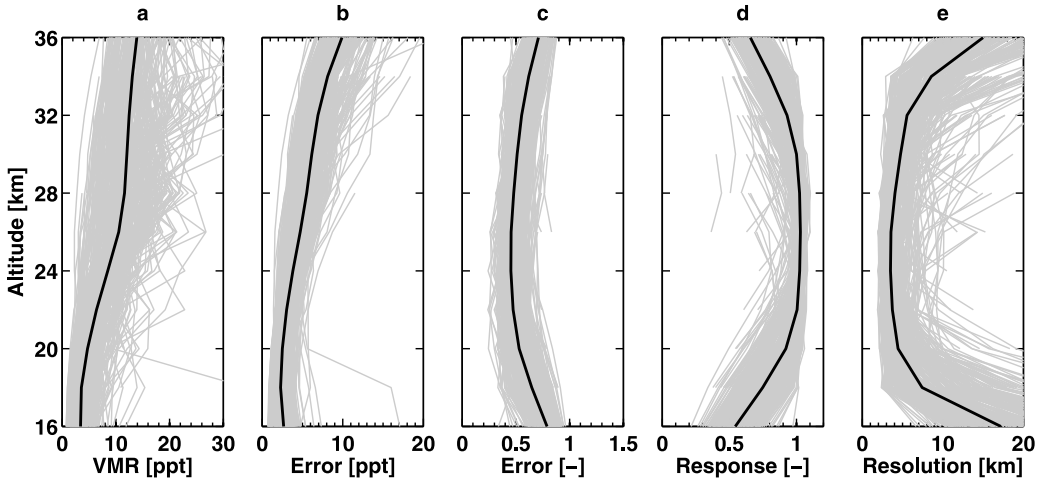

Figure 5. Characteristics of the OSIRIS BrO data set. Light grey lines are individual retrievals (every 100th profile shown), and thick black line is the median value considering all latitudes and both local times: (a) mixing ratio, (b) absolute retrieval error, (c) fractional retrieval error, (d) response, and (e) resolution.

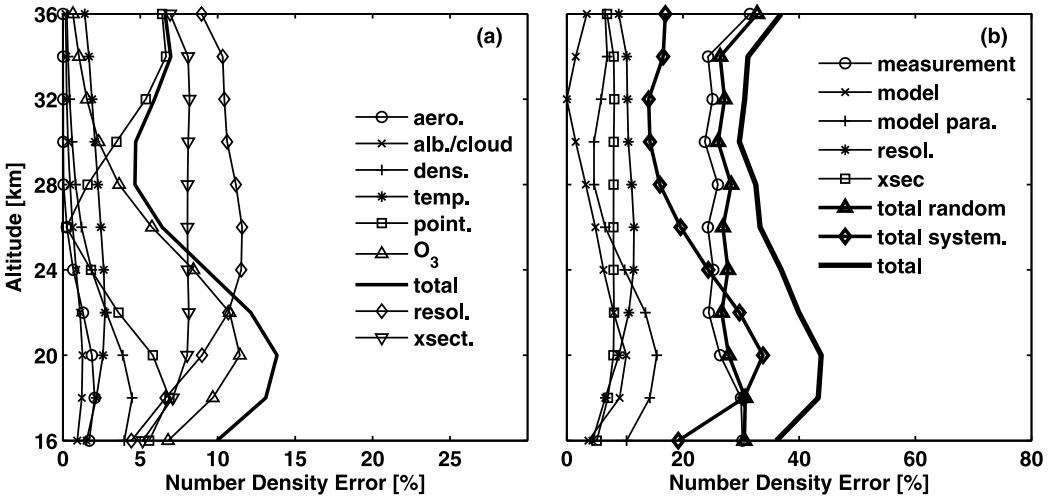

Figure 6. Results of error analysis using synthetic spectra for a SZA of 85°, a change in azimuthal angle of 90°, and surface albedo of 0.3. (a) Forward model parameter errors due to uncertainties in aerosol, surface albedo/cloud, neutral density, temperature, pointing, and O_3 profile, given as 1 standard deviation (STD), and the total forward model parameter error, obtained by adding the individual source in quadrature. Also shown (but not included in the total) are errors due to spectral resolution and the BrO cross section. (b) Measurement, forward model, forward model parameter, spectral resolution, and BrO cross-section errors. Total random error is calculated by adding the measurement and spectral resolution terms in quadrature. Total systematic error is calculated by adding the forward model, forward model parameter, and BrO cross-section terms. The total overall error is calculated by adding the total random and systematic in quadrature.

is typically 3–5% and never exceeds 10% for BrO retrievals. The forward model parameter error was assessed by perturbing a model parameter by its typical uncertainty in the forward simulation and then performing a retrieval using the standard value. Again, the procedure of *Haley et al.* [2004] was followed. Here the individual sources were added in quadrature as they were assumed to be independent. Results are shown in Figure 6a. The largest sources are OSIRIS spectral resolution, or slit width, which was perturbed by 5% (this is discussed further is section 3.7) and BrO cross-section errors. In the error budget these two sources were treated separately from the other forward model parameter errors and thus were not included in the calculation of the total model parameter error curve in Figure 6a.

[30] The forward model parameter error considered an error in the assumed ozone profile. Errors in the absorption spectra of interfering species, of which ozone is the most important, were not considered. This error source was difficult to assess as only an error in the spectral structure is relevant. Care was taken to minimize this error source by allowing for a relative shift in wavelength between the reference ozone spectra and OSIRIS. Further, ozone cross sections at three temperatures were included in the spectral fit. Preliminary sensitivity tests indicated that the use of an ozone cross section measured at an temperature that differs significantly from the effective atmospheric temperature may lead to profile errors of up to a factor of two.

[31] The smoothing error arises because of the limited vertical resolution of the retrieval and the nonzero correlation length in the a priori covariance matrix. Retrieval noise represents the error source due to noise on the radiances, propagated through the retrieval, and is dependent on the a priori covariance matrix. The covariance matrix was constructed on the basis of box model simulations of BrO with an uncertainty of 100% and an ad hoc correlation length of 4 km, implemented as a smoothing constraint. As these were not based on an observed ensemble of states, the resultant smoothing error had little meaning. As a result we do not consider smoothing error in the error budget, but rather consider the retrieval to be an estimate of a smoothed version of the true state as suggested by *Rodgers* [2000].

[32] A plot of the error categories is given in Figure 6 and summarized in Table 1. Values in Table 1 are representative of the 24–32 km, the portion of the BrO profiles that are the most robust. The largest error source was the retrieval noise with values near 25%. Other sources were in the 5–10% range. To determine the total error, a distinction between random and systematic sources of error was made. Model errors and model parameter errors are generally considered systematic errors, including the error in BrO cross section. An exception to this is the slit width, or resolution, error. As described in section 3.7, when OSIRIS temperatures depart from nominal values, the slit width, or resolution, is affected. A robust correction is applied such that retrievals, in a monthly mean sense, make use of the slit width appropriate for that monthly mean instrument temperature. Thus, any remaining slit width error, estimated to be 5%, can be considered random. Adding the random errors in quadrature gave a total random error, or precision, of about 27%. The simple sum of the systematic errors, or bias, is 17%. For individual BrO profiles, random and systematic errors may be added in quadrature for a total error of 32%. It is reiterated here that as a result of not being able to quantify the smoothing error, this error budget is appropriate for a smoothed version of the true state. When monthly means of BrO are considered, the random error component becomes

Table 1. Error Budget[a]

Error Source	Type	Magnitude (%)
Retrieval noise	R	25
Forward model parameter		
Resolution	R	10
All others	S	6
Forward model	S	3
BrO cross section	S	8
Total BrO systematic		17
Total BrO random		27
Inferred precision, Figure 11		~30
Total BrO Error		32
Photochemistry	S	7
Br_y systematic error		24

[a]Error type is either random (R) or systematic (S). Random errors were added in quadrature. The total error in BrO was obtained by adding the total random and total systematic errors in quadrature.

small and the systematic component becomes the dominant source.

[33] As mentioned in section 3.3, photochemical box model calculations were used to map the OSIRIS BrO to the local time of another instrument to facilitate a comparison or to derive total Br_y. In each application this introduces an additional source of systematic error, called photochemical error. Photochemical error includes errors in the box model constraints such as the prescribed ozone, temperature, or families, and rate constants. *Sioris et al.* [2006] found that the key components in the photochemical error are in the assumed values of air density, NO_2, and the rate coefficients of the primary formation and destruction reactions,

$$\text{(R3)} \qquad BrONO_2 + h\nu \rightarrow BrO + NO_2$$

$$\text{(R4)} \qquad BrO + NO_2 + M \rightarrow BrONO_2 + M$$

Following *Sioris et al.* [2006], the photochemical error was assessed by successively varying air density, NO_2, and the reaction rate coefficients by their uncertainty, and then recomputing BrO in the box model for a tropical and midlatitude scenario. The photochemical error is the sum of these, added in quadrature. An error of 7% is representative of altitudes above 20 km for OSIRIS AM BrO and all altitudes for OSIRIS PM BrO. Below 20 km, AM errors were found to be larger, up to 40%, due to uncertainties in the photolysis rate coefficient of reaction (R3). The abundance of BrO is very sensitive to the rate of release from $BrONO_2$ following its buildup throughout the night. Photochemical error is treated as a systematic source.

3.7. Observations During Eclipse Season

[34] Every year between May and July, Odin spends a significant fraction of its orbit in eclipse, with this fraction peaking in June. This results in a gradual cooling of the spacecraft. Sensors in the OSIRIS optics indicate that the temperature drops from a nominal value of 22°C to a minimum of about 10°C. This acts to (1) induce a small wavelength shift, (2) blur the image as manifested by an increase in the slit function width, and (3) introduce a TH offset [*McLinden et al.*, 2007]. This last effect is brought about by a thermal flexing of the spacecraft which alters the alignment of OSIRIS relative to the star tracker, from which OSIRIS obtains its pointing information. Each effect represents a potential source of additional error in the BrO retrievals. The 2001–2008 time series of monthly mean optics temperatures is shown in Figure 7a. While the eclipse period lasts from May–July, there appear to be some lingering effects through to September.

[35] For each zonal mean scan the spectral fitting algorithm determines any relative wavelength shift between the OSIRIS spectra and the cross-section data. During eclipse periods, OSIRIS wavelengths were found to be blue-shifted by about 0.1 nm, corresponding to about one quarter of an OSIRIS pixel. However, the calculated shift was applied to the OSIRIS spectra and thus eliminated the wavelength shift as a potential error source.

[36] Prelaunch testing suggested that a decrease in the OSIRIS optics temperature from 22°C to 10°C leads to a 20% increase in the slit width. As seen in Figure 6, a 5% increase in the slit width leads to an underestimation of BrO in the neighborhood of 10%. In other OSIRIS data products such as NO_2 this effect was much smaller, about 3% [*Haley et al.*, 2004], and so was ignored. The reason for the increased sensitivity in BrO is primarily from the interference of O_3 in the spectral fitting. To account for this, the cross-section data (and pseudo-absorber basis functions) were generated for a set of slit width scalings: 0.9, 0.95, 0.975, 1.0, 1.025, 1.05, 1.1, 1.15, 1.2, 1.3 and 1.4, and an expression relating optics temperature, T_{opt}, to relative slit width, w, based on the prelaunch test data was derived,

$$w = 0.8936 + 0.1064 \exp\left[-0.0819\left(T_{opt} - 22\right)\right] \qquad (1)$$

where T_{opt} is in °C and gives a value for w of 1 for $T_{opt} = 22$°C and 1.18 for 10°C. On the basis of the optics temperature for a given scan, the cross sections calculated for the nearest slit width scaling were used in the inversion. Values of w for monthly mean optics temperatures are shown in Figure 7b. The standard (scaling of 1) cross sections were generally used for data from October–April. Data from May–August use reduced resolution cross sections with September somewhere between. Future data versions may employ an alternative approach in which the relative slit width is calculated from measured spectra.

[37] The final eclipse effect, a TH offset of up to 500 m, has been observed in comparisons between OSIRIS ozone and ozonesondes [*McLinden et al.*, 2007]. This leads to a systematic error in the retrieved BrO of 0–6% as seen in Figure 6 with opposite signs at the top and bottom of the profile. Given its relatively small error contribution, no correction was applied for this effect in the current data version.

4. BrO Climatology

[38] OSIRIS BrO monthly means have been calculated using the full 7+ years of data from November 2001 to December 2008. Averages were computed using the same altitude, latitude, and AM/PM binning as the zonal mean L1 spectra. Individual data points with a response of 0.67 or smaller or a relative error of 100% or greater have been excluded. A response threshold of 0.67 was chosen to ensure data points that are heavily influenced by a priori information are excluded [*Urban et al.*, 2005]. Because of

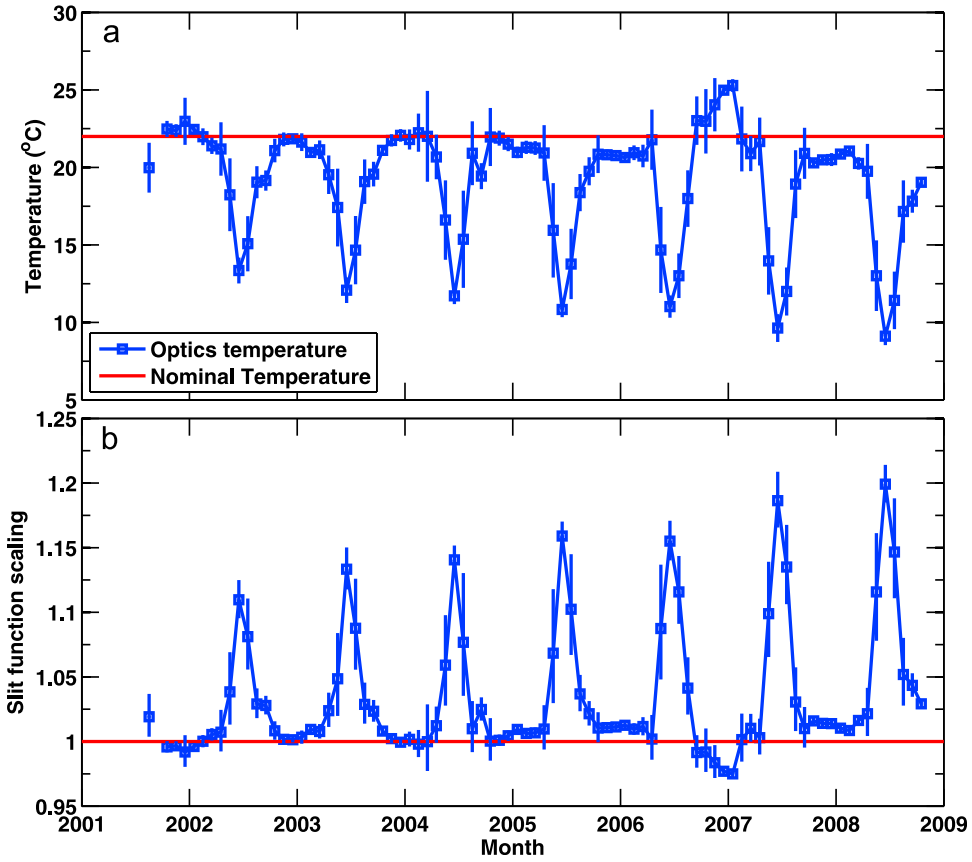

Figure 7. (a) Time series of monthly mean OSIRIS optics temperature. Errors bars denote the standard deviation. (b) Relative slit function scaling, *w*, calculated using monthly mean temperatures from Figure 7a in equation (1). Error bars show range in scaling using the mean ±1-STD optics temperature. The red lines show the nominal values.

the steep gradients near sunrise and sunset, BrO is particularly susceptible to diurnal effect errors, or the diurnal variation in BrO along the line of sight due to a changing local SZA [*McLinden et al.*, 2006]. To minimize the impact of this error source, only SZAs of 87° or smaller were included in the monthly means. Finally, only mean values made up of at least 20 individual data points were considered. After this filtering, monthly mean profiles typically extend from 16 to 34 km in the tropics and 18–36 km in the extratropics.

[39] Figure 8 shows the resulting monthly mean AM (descending node) BrO (BrO-AM) maps. There is a minimum of 3 pptv at the tropical tropopause and an increase with altitude and poleward to a maximum of about 16 pptv. Some seasonal features can be understood by examining OSIRIS monthly mean NO_2 number density [*Brohede et al.*, 2007b], shown in Figure 9 (also calculated using SZAs of 87° or less).

[40] Because of the coupling of the nitrogen and bromine families via reactions (R4) and (R3) there is expected to be a relationship between BrO and NO_2. Months such as March and October show a local maximum in BrO around 24 km in the north polar region that can be attributed to the minimum in NO_2 due to its conversion to NO_y reservoir species, thereby making it unavailable to form $BrONO_2$. (It is expected that a similar feature would be present through the NH winter.) Likewise, in the NH summer, the BrO contours are much wider indicating reduced values. Again this is consistent with the NO_2 which shows a maximum in this region. An overall seasonal cycle is also evident with a maximum in the winter pole and a minimum in the summer pole. This is related to the seasonal cycle in NO_2 and is consistent with the findings of *Pundt et al.* [2002].

[41] A BrO-NO_2 correlation plot is shown in Figure 10 at a latitude of 65°N where there is a large seasonal cycle and 8 months of coverage. Correlation coefficients in the lower stratosphere (16–26 km) were typically −0.9 where the coupling is expected to be tight, but above this values were small and slightly positive. At 34 km, for example, BrO is completely unaffected by the NO_2 seasonality. The reduced sensitivity to NO_2 above 30 km is a result of the rapid decrease in the production rate of $BrONO_2$, reaction (R4), from the declining densities of NO_2 and air.

[42] The monthly BrO AM standard deviations, expressed as a fraction of the mean, are shown in Figure 11. Values between 0.2–0.35 dominate, with occasional pockets up to 0.5. The larger standard deviation at the South pole from September to November below 20 km is likely due to differing amounts of denitrification from year to year. The other pockets of higher standard deviation tend to coincide with smaller absolute amounts of BrO. In general, sources of

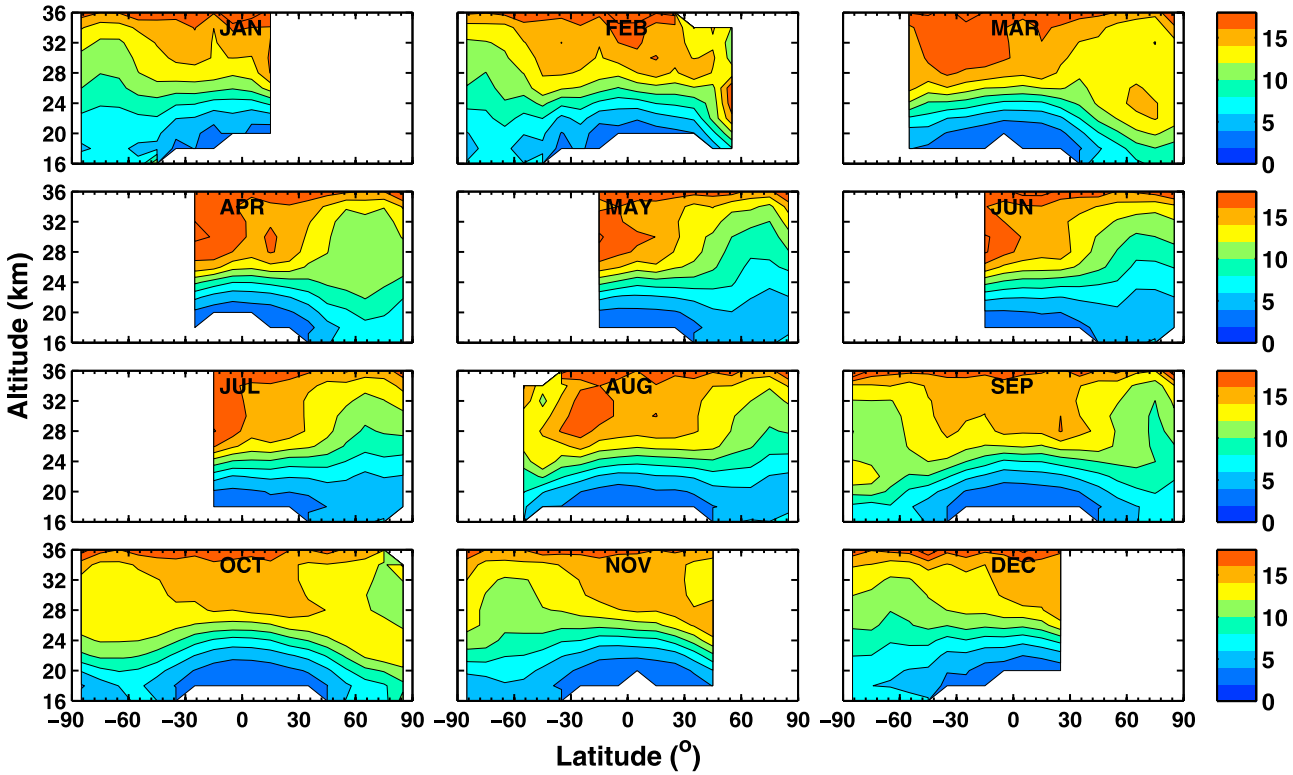

Figure 8. OSIRIS monthly mean descending node (AM) BrO mixing ratio (in pptv), averaged over November 2001 to December 2008.

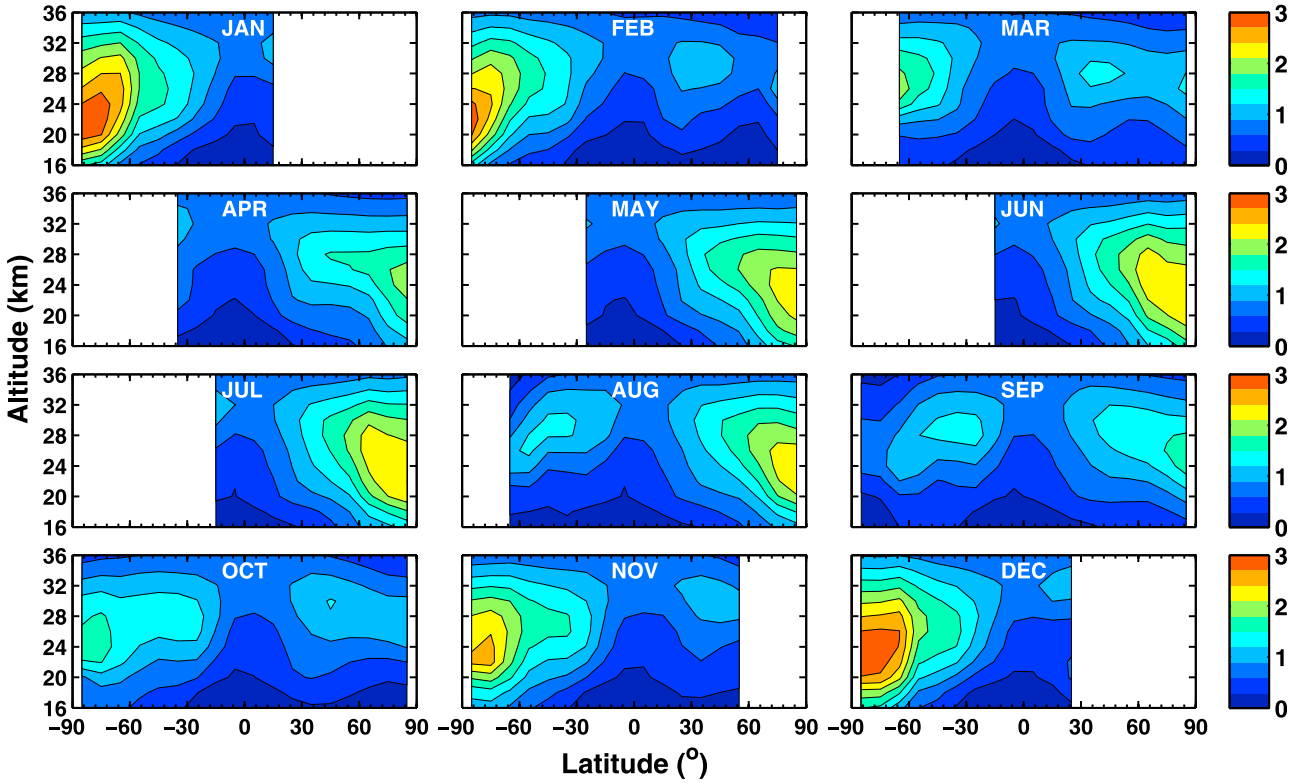

Figure 9. OSIRIS monthly mean descending node (AM) NO_2 number density, averaged over November 2001 to December 2008.

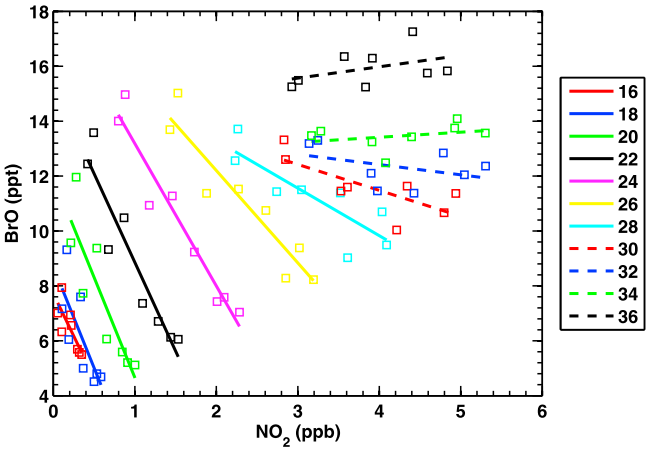

Figure 10. Correlation between OSIRIS monthly mean ascending node (AM) BrO and NO_2 at 65°N at each retrieval altitude as indicated in the legend (km). Each square represents a monthly mean value. The lines represent least-squares fits to the data.

variability include natural day-to-day, interannual variability, a drifting of the Odin orbit in LST, and noise in the retrieval. The contribution from Odin's drift in LST can be assessed by examining the monthly standard deviations of the a priori profiles. Removing this from the retrieved BrO standard deviations leads to a 3–5% reduction. Considering all this, the precision (random error) of a typical daily profile can be considered to be ~30%. This can be contrasted with the theoretical precision estimate of 27% from Table 1.

[43] Since Odin possesses a sunrise-sunset orbit, OSIRIS has the advantage of measuring at two local times (~0630 and 1830), although because of the precession of Odin's orbit toward later local times, the AM half of the orbit is favored with little or no PM coverage in the tropics from about 2004 onward. Coverage is further limited by the SZA limit of 87°. As a check of the internal consistency of the OSIRIS BrO product, AM-PM monthly mean differences were calculated and compared to monthly mean a priori differences (not shown). There is a consistent month-to-month picture, with generally larger mixing ratios in the AM for northern extratropics but more of a mixture in the southern extratropics. Since SZAs are smaller in the northern hemisphere summer than the southern hemisphere summer, this hemispheric difference is not necessarily unexpected.

5. Comparisons With Other Instruments

5.1. Diurnal Mapping

[44] Because of its diurnal nature, comparisons between instruments measuring BrO at different local times must be made with caution. As was done for the validation of OSIRIS NO_2 [*Brohede et al.*, 2007a] as well as ACE-FTS NO and NO_2 [*Kerzenmacher et al.*, 2008], in this work OSIRIS BrO was mapped from its local time to that of the

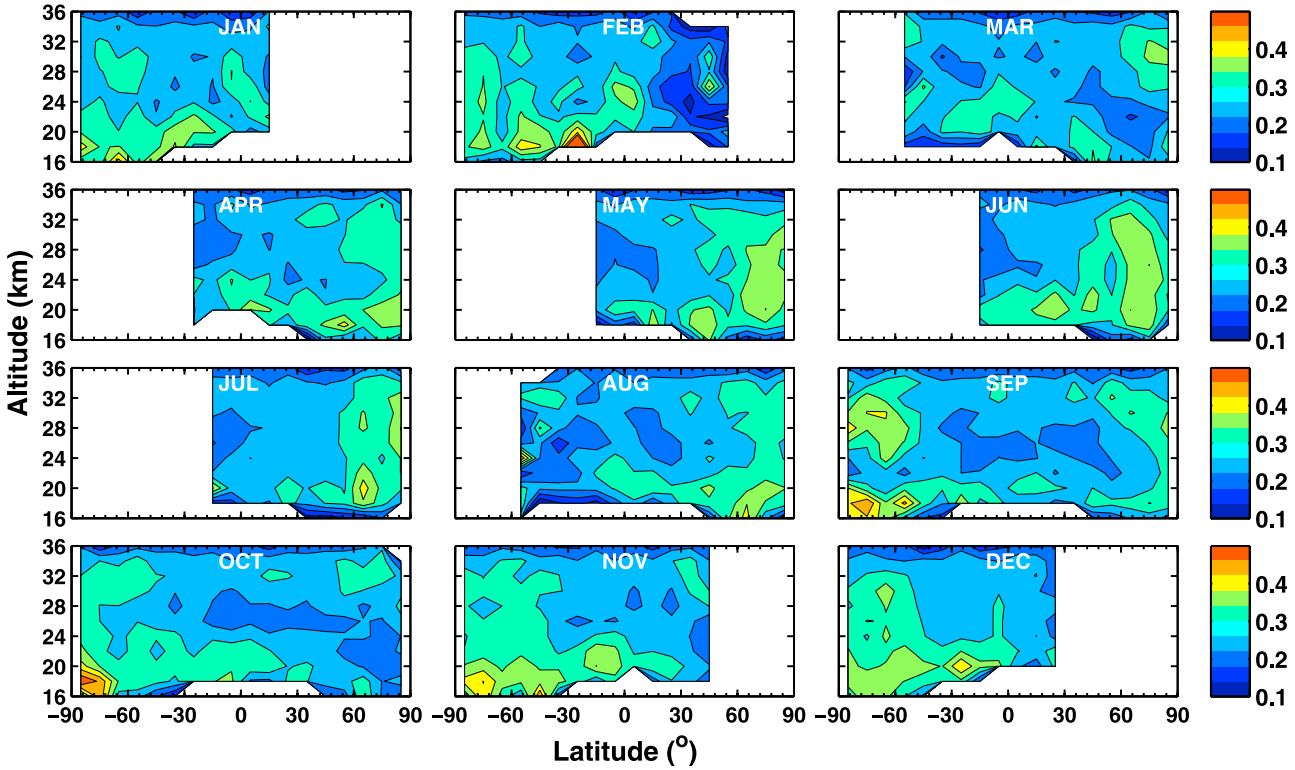

Figure 11. Standard deviation (1 STD) of OSIRIS monthly mean descending node (AM) BrO (expressed as fraction of the mean), averaged over November 2001 to December 2008. Results for ascending node (PM) BrO are similar.

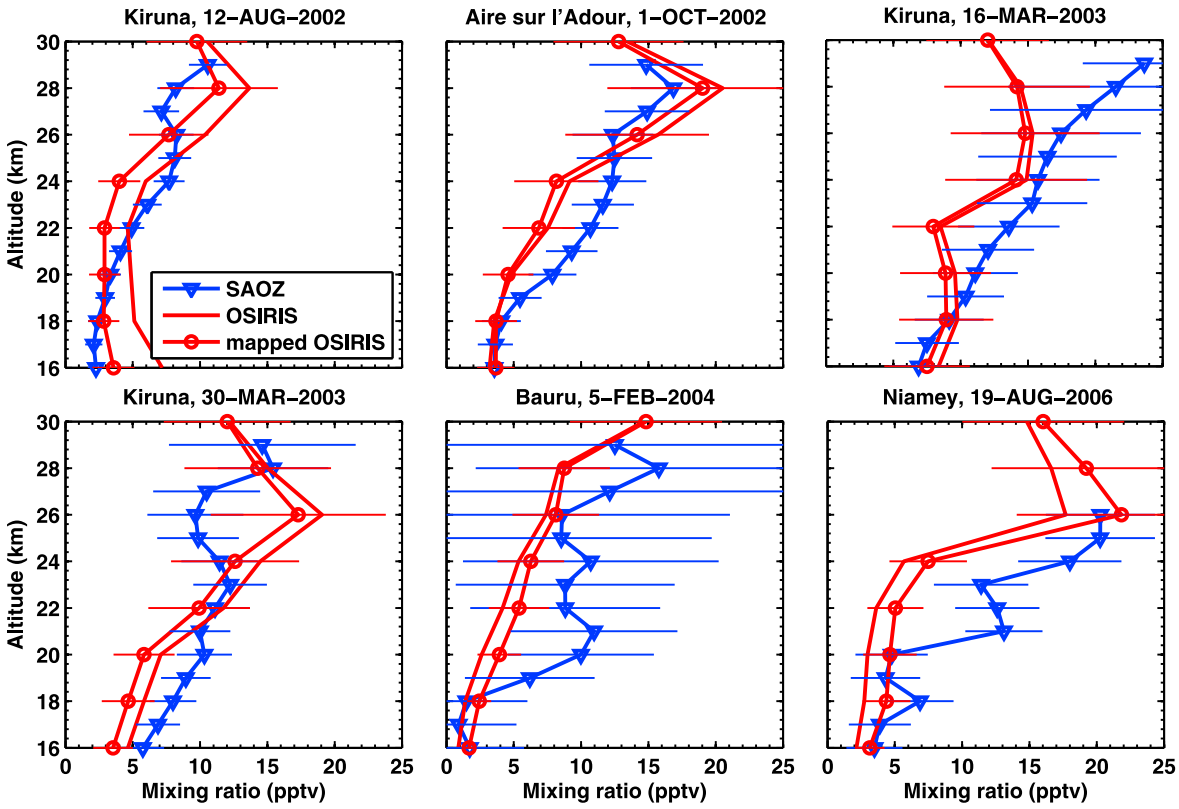

Figure 12. Comparison between Systeme d'Analyse par Observations Zenithales (SAOZ)–BrO balloon profiles and OSIRIS daily, zonal mean profiles at Kiruna, Sweden (68°N), Aire sur l'Adour, France (44°N), Bauru, Brazil (22°S), or Niamey, Niger (13°N). Shown are the original OSIRIS profiles (solid) and OSIRIS mapped to the SAOZ SZA (solid+circle). OSIRIS error bars represent the all error sources in Table 1. The error bars on the SAOZ profiles are the one standard deviation errors of the spectral fitting propagated in the profile retrieval process. Their amplitude is highly dependent on the SZA at which the flight was performed, between 83–87° for most of the flights, but that of Bauru at 75°.

correlative instrument. This was done using box model calculations using the following expression:

$$n_{OS}(LST_i) = n_{OS}(LST_{OS})\left[\frac{n(LST_i)}{n(LST_{OS})}\right]_{model} \quad (2)$$

where n is the BrO number density and the subscripts "OS", "i", and "model" represent OSIRIS, other instrument, and box model, respectively. For single-profile comparisons the box model is constrained with ECMWF temperature and simultaneously measured OSIRIS ozone [*Haley and Brohede*, 2007], averaged over the same scans that were used in deriving the zonal L1 data, as well as monthly mean Odin NO_y [*Brohede et al.*, 2008]. When monthly means were compared, the box model was initialized with monthly mean ECMWF temperature, OSIRIS ozone, and Odin NO_y. This assumes the partitioning of Br_y among its family members is largely independent of the absolute amount of Br_y specified.

5.2. Single Profile Comparisons

[45] The zonal mean nature of OSIRIS BrO means it is difficult to derive quantitative information when comparing to single BrO profiles. Nonetheless, it is still worthwhile given the limited sources of correlative BrO profiles. OSIRIS BrO was compared with profiles measured from the SAOZ-BrO balloon-borne instrument [*Pundt et al.*, 2002], a UV spectrometer designed specifically to measure BrO via solar occultation during the ascent of the balloon. Comparisons were only considered if OSIRIS measurements exist for the same day, within 5° latitude of a SAOZ profile, and if the individual scans contributing to the zonal L1 spectra bracketed the SAOZ longitude. Six OSIRIS-SAOZ profiles matched these criteria, and they are shown in Figure 12. The common altitude range is 16–30 km. These SAOZ profiles were recorded in the late afternoon between SZAs of 83–87°. Both the original OSIRIS profile and the OSIRIS profile mapped to the SZA of SAOZ are shown. Overall there is a general consistency between the two profiles, with some larger differences where the error bars do not overlap, particular for the Niamey comparison. However, it is difficult to differentiate between actual inconsistencies and those differences caused by the instruments viewing differing air masses. All mapped OSIRIS profiles agreed better with SAOZ than did the originals.

5.3. Monthly Mean Profile Comparisons

[46] Comparisons of monthly mean OSIRIS profiles were made with those from SCIAMACHY, a satellite

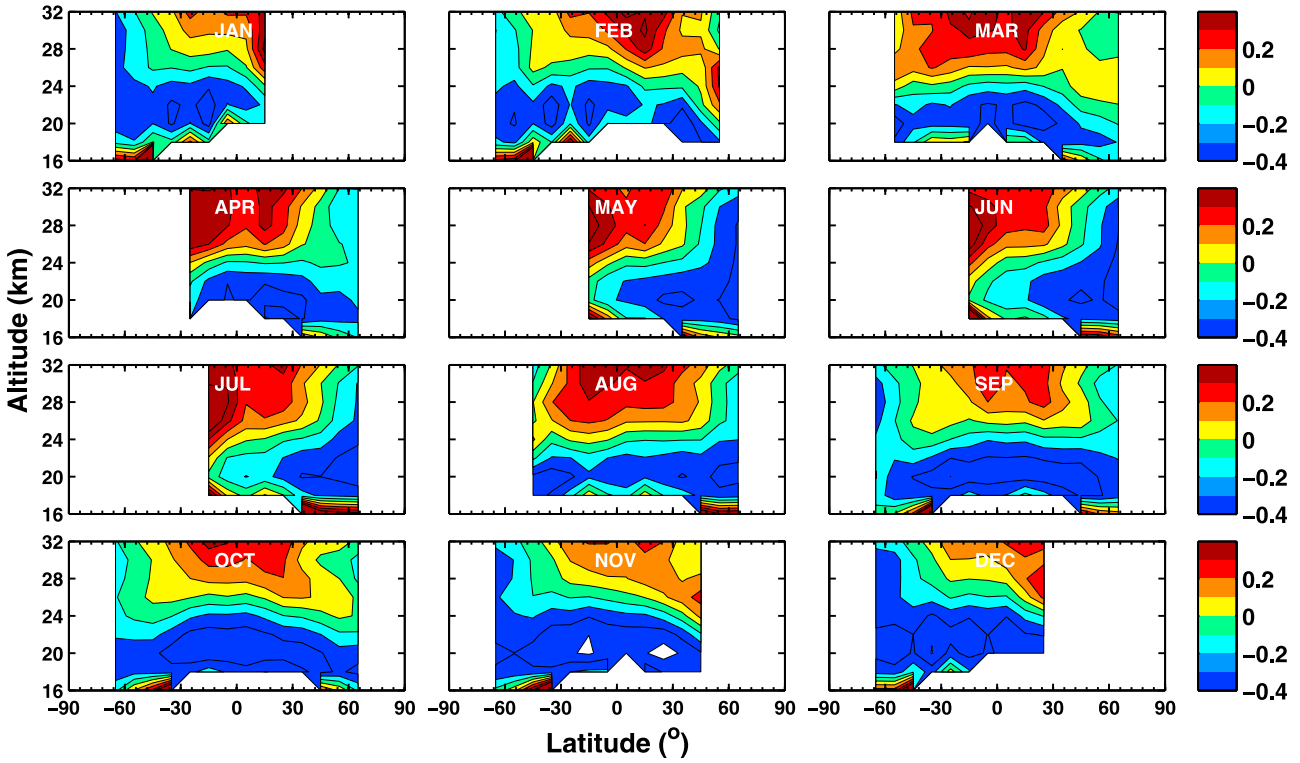

Figure 13. Relative difference between OSIRIS-AM (2001–2008) and SCIAMACHY (2002–2008) monthly mean BrO, calculated as (OSIRIS-SCIAMACHY)/SCIAMACHY. OSIRIS means have been mapped to the local time of the SCIAMACHY observations.

instrument on-board ENVISAT [*Bovensmann et al.*, 1999]. SCIAMACHY, like OSIRIS, measures BrO profiles using limb-scattered sunlight [*Sinnhuber et al.*, 2005]. The relative difference between OSIRIS BrO-AM and SCIAMACHY monthly means, with OSIRIS interpolated to the SCIAMACHY grid and mapped to the LST of ENVISAT (~1000), is shown in Figure 13 over their common retrieval range, 16–32 km. Latitudes poleward of 70° were excluded as the SCIAMACHY BrO in these regions may be subject to large diurnal effect errors. The relative difference was calculated using (OSIRIS-SCIAMACHY)/SCIAMACHY. All months tended to display a similar pattern with OSIRIS larger in the topics above about 26 km. Poleward and below this SCIAMACHY BrO tends to be larger. Contrasting the differences in the NH between June and October, it is clear that OSIRIS possesses a stronger seasonal cycle than SCIAMACHY. This could be attributed to an incomplete removal of the eclipse effect, but if that were the case it should also be visible at tropical latitudes, which is not. In the lowest OSIRIS retrieval altitudes, where there may be some edge effects. The overall level of agreement between the two monthly mean data sets is in the 30–40% range. This can be compared with the estimate of OSIRIS systematic errors, about 25% including a photochemical contribution.

[47] A comparison with profiles derived from ground-based zenith-sky UV-visible spectrometers at Harestua, Norway (60°N), and Observatoire de Haute-Provence (OHP), France (44°N), has also been conducted. Details of the retrieval algorithm are available elsewhere [*Hendrick et al.*, 2008], but in short, it uses a combination of spectral fitting to obtain SCDs and optimal estimation to invert the SCDs to number density profiles in conjunction with a radiative transfer model and a photochemical box model. The resolution of the profiles is rather coarse at ~10 km with roughly two independent pieces of information in the stratosphere [*Hendrick et al.*, 2007]. The Harestua data set used in this study spans 2002–2006, very close to the OSIRIS coverage. OHP is shorter, 2005–2006. Monthly mean Harestua total VCDs were found to be in good agreement with SCIAMACHY and Global Ozone Monitoring Experiment (GOME) VCDs. The comparison of OSIRIS monthly means (average of 55° and 65°N) with the Harestua monthly means is shown in Figure 14 for the 8 months of OSIRIS coverage at this latitude. OSIRIS profiles have been mapped to a SZA of 80° and then convolved with the *Hendrick et al.* [2007] averaging kernels. The comparison was generally consistent with that of SCIAMACHY in that in the summer months, OSIRIS was consistently smaller, by up to 25%, but for March and October, there is excellent agreement. The comparison with OHP was very similar (not shown).

6. Implication for Total Br_y

[48] A number of recent studies have attempted to quantify the total amount of inorganic bromine in the stratosphere, and hence the contribution from VSLS. These include ground-based UV-vis instruments [*Hendrick et al.*, 2007], the balloon-borne DOAS/LPMA [*Dorf et al.*, 2006, 2008], MLS/Aura [*Kovalenko et al.*, 2007], SCIAMACHY from two different research groups [*Sinnhuber et al.*, 2005; *Sioris et al.*, 2006], and a balloon-borne whole-air sampler [*Laube et al.*, 2008]. The *Laube et al.* [2008] measurements

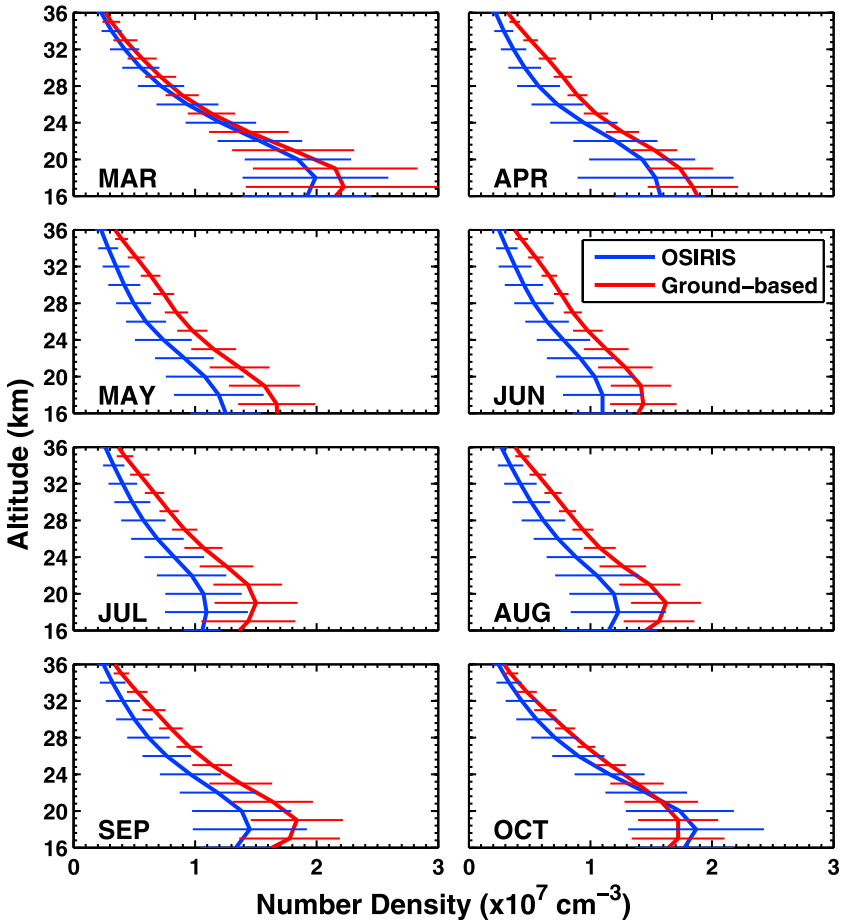

Figure 14. Comparison of monthly mean OSIRIS (AM) and ground-based AM BrO profiles from Harestua, Norway (latitude = 60°N). Error bars represent the standard deviation of individual profiles. OSIRIS BrO is the mean of the 55°N and 65°N monthly mean profiles and has been mapped to the SZA of the ground-based profiles (80°).

differ from the others in that bromocarbons are measured in situ throughout the upper troposphere and stratosphere. These estimates vary from 17.5 to 25 pptv and are based on measurements made after 2000, and hence probe air entering the stratosphere after ~1995. Between 1995 and 2005 the sum of CH_3Br and the halons delivered into the stratosphere has been roughly constant at 15.5–17 pptv due to an offsetting decline in CH_3Br and increase in halons, with a peak in 1998 [*WMO*, 2007]. As such, to a first approximation, it is fair to compare these results with OSIRIS without regard to year of measurement or age of air. If the contribution of CH_3Br and halons to total Br_y is taken at 16 pptv over this period, then this would imply a VSLS source of 1.5 to 9 pptv. This can be compared with the *Laube et al.* [2008] measurements of organic bromocarbons in the tropical tropopause layer which suggested a contribution from VSLS of 1.3 pptv. These varied results highlight the uncertainty in the VSLS contribution to Br_y.

[49] In this section, two methods were used to obtain an estimate of total stratospheric Br_y. The first involves comparing OSIRIS partial VCDs to those predicted by the photochemical box model initialized with different amounts of VSLS. A similar approach was used by *Salawitch et al.* [2005] and *Sioris et al.* [2006]. The box model was run for the 15th of each month and constrained with monthly mean ECMWF temperature, OSIRIS ozone, SMR N_2O, and Odin NO_y. VCDs were calculated but restricted to the common OSIRIS retrieval range over all latitudes: 20–34 km. This also ensured that only the highest retrieval responses were used. All scenarios used the Wamsley "organic" Br_y expression, updated to 2005 (the midpoint of the OSIRIS data set), but with a VSLS contribution, constant with altitude, such that the total Br_y is varied from 19 to 25 pptv in 1 pptv increments. Adding a constant amount of Br_y at all altitudes assumes the source is short-lived and releases its bromine (or, converted to inorganic form) in the lowermost stratosphere. It also assumes that there is no trend in the source since it is constant with age of air.

[50] Results for the month of September are shown in Figure 15a. Calculating the minimum RMS differences over latitude for the different scenarios suggested the best agreement was for total Br_y of 21–22 pptv. This value was further refined by fitting a quadratic to the three smallest RMS values and finding the Br_y amount that minimized the RMS quadratic. For September this gave a values of 21.1 pptv. Analogous values for all months are shown in

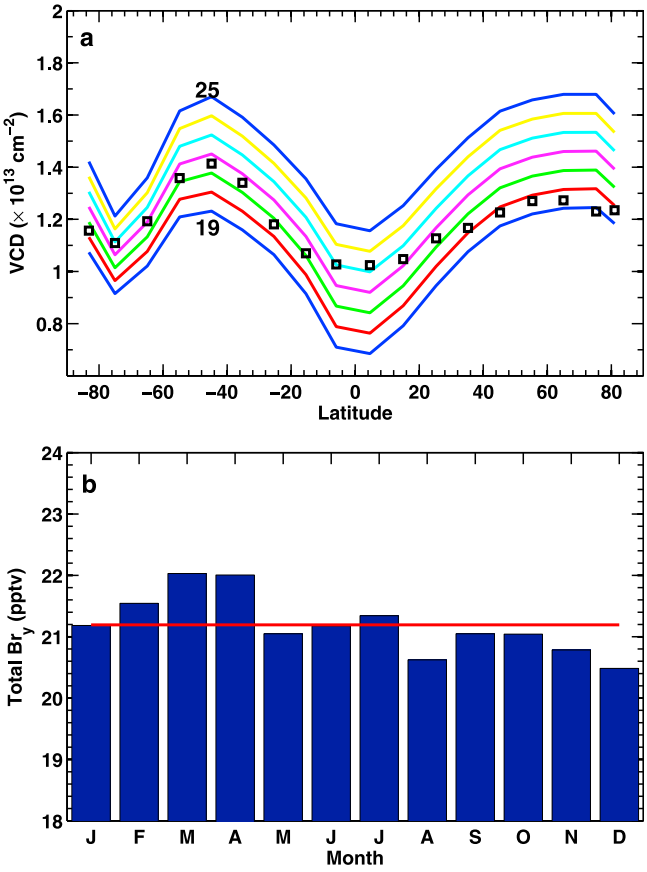

Figure 15. (a) Comparison of monthly mean OSIRIS BrO (AM) partial vertical column densities (VCDs) (19–35 km) to those from a photochemical box model assuming varying levels of Br_y contribution from very short lived substances (VSLS) for September. Solid lines show model calculated partial VCDs for a total Br_y of 19–25 pptv (19 and 25 pptv values are indicated with blue lines; other colors represent intermediate values in 1 pptv increments), and squares indicate OSIRIS values. Considering all latitudes, a total Br_y of 21.1 pptv best agrees with the OSIRIS partial VCDs. (b) Inferred total Br_y for each month. The horizontal line indicates the mean over all months, (21.2 ± 0.5) pptv.

Figure 15b. All months had values from 20–22 pptv, including the summer months, which suggested that the algorithm used to correct the varying OSIRIS slit width was appropriate. The mean Br_y over all months is 21.2 pptv with a standard deviation of 0.5 pptv. An advantage of this method in assessing the VSLS contribution, as opposed to only using altitudes at which the organic sources species have completely released their bromine (i.e., 30+ km), is that the full profile is used thereby minimizing random errors. However, it assumes the shape of the Br_y profile is known, to within a constant offset.

[51] The second method of estimating total Br_y was to derive it directly from BrO using photochemical modeling. In this work, Br_y was derived from the monthly mean BrO from section 4 using the expression,

$$n_{OS}^{Br_y} = n_{OS} / \left[\frac{n}{n^{Br_y}}\right]_{model} \quad (3)$$

analogous to the method employed by *Kovalenko et al.* [2007] and numerous other studies. The BrO/Br_y ratio was calculated using the photochemical model set to the midpoint of each month and constrained with monthly mean OSIRIS O_3, ECMWF temperature, SMR N_2O, and Odin NO_y. Once an initial estimate of the Br_y was obtained, it was then used in the box model to recalculate BrO/Br_y in case the partitioning was sensitive to the assumed Br_y profile. Monthly Br_y calculated in this fashion from the BrO-AM data are shown in Figure 16. The morphology is similar to BrO but with reduced seasonality. Some seasonality is expected given the Brewer-Dobson circulation pattern. There is a plateau of 18–22 pptv above 28 km or so, with some months displaying the maximum in the tropics, others in the extratropics. The extratropics also show a small decline above the peak which may be an age-of-air effect. The uppermost retrieval level often shows a 1–2 pptv jump, similar to that seen in BrO, which appears to be an artifact of the retrieval related to the amount of BrO assumed above the top of the retrieval range. In some instances, too little BrO may be assumed above the 36 km, and thus the BrO in the uppermost retrieval level is forced to compensate.

[52] OSIRIS monthly Br_y, from Figure 16, was examined in tracer space in Figure 17. This shows the correlation between monthly mean SMR N_2O and OSIRIS Br_y, considering latitudes between 40°S to 40°N. Tracer space offers the advantage of reducing differences due to age of air. Figure 17a shows the individual OSIRIS monthly Br_y data points for both AM and PM as well as their values averaged over 20 ppbv-wide N_2O bins. The values at the smallest N_2O occur at altitudes of 36 km, and these may be subject to some top of retrieval range effects. Overall the AM and PM are generally similar, and the differences that exist are likely related to the difference in latitudinal sampling with most of the PM coverage originating from the 25° and 35° latitude bins. Figure 17b shows the bin-averaged N_2O-Br_y correlation along with the *Wamsley et al.* [1998] "organic" relationship, which considers only CH_3Br and halons, adjusted to 2005 as follows. In the tropics the mean age of air over the OSIRIS retrieval range is ~3 years. Hence the Br_y maximum in the *Wamsley et al.* [1998] relationship is scaled to 16 pptv, a value obtained from *WMO* [2007] for 2002, the year of stratospheric entry. In Figure 17b the mean Br_y over all AM and PM monthly values are used. Given the much larger number of AM measurements in this latitude range, about 3 times the PM, the overall mean is heavily weighted toward the AM mean from Figure 17a. Correlations from MLS and a DOAS balloon flight are also shown, taken from *Kovalenko et al.* [2007], as are total Br_y estimates from other sources and shown simply as open triangles. The OSIRIS correlation is very similar to the MLS and DOAS curves. By taking the difference between the OSIRIS and Wamsley curves, an estimate of the Br_y originating from VSLS can be made. This difference was 5 pptv on the low-N_2O end and 7 pptv on the high end. The simple mean of these values is 5.8 pptv.

[53] The inferred OSIRIS Br_y from the correlation plot, representative of 2005, is 21.0 pptv, chosen as it is the maximum value (outside of the data point corresponding to 36 km, or low N_2O, which may be contaminated by a

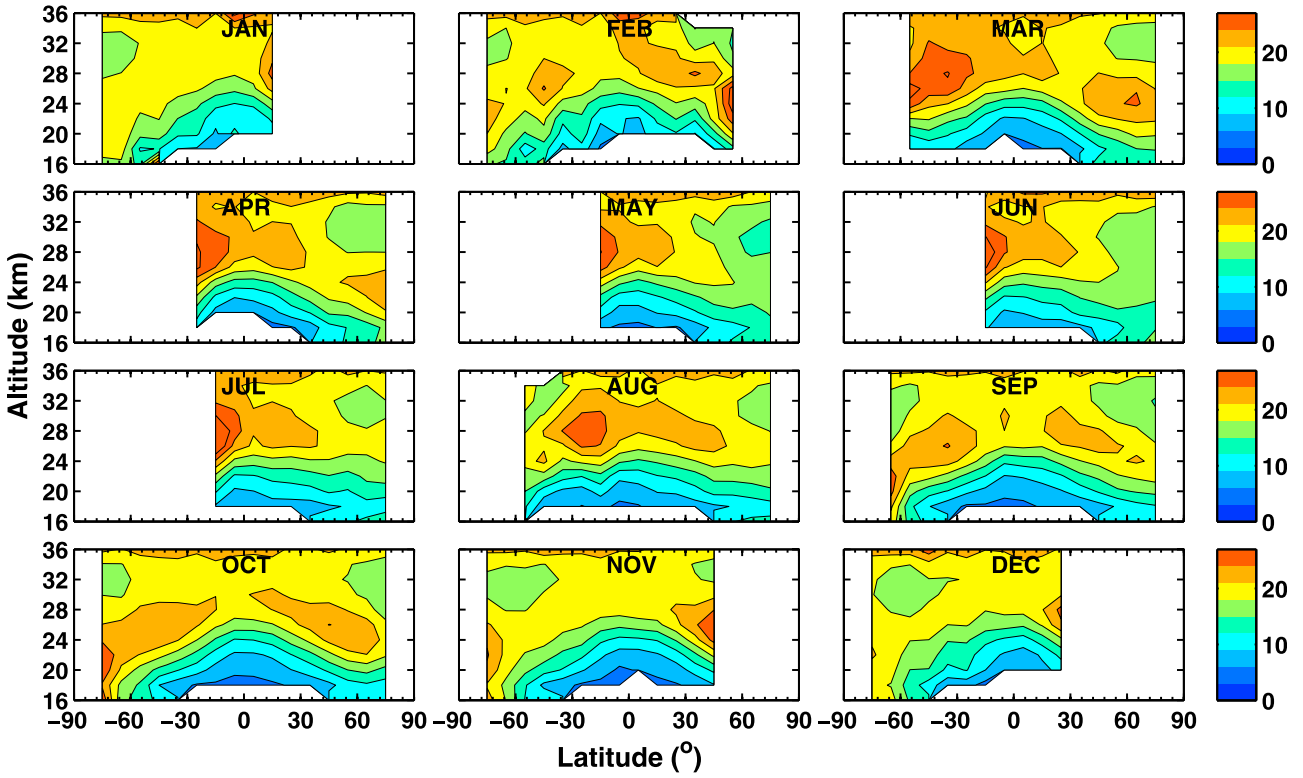

Figure 16. OSIRIS monthly Br_y (in pptv) calculated from descending node (AM) monthly mean BrO shown in Figure 8.

retrieval artifact). This is virtually identical to the 21.2 pptv obtained from the column method. The slow decline with altitude just above this (decreasing N_2O) appears consistent with an age of air effect. A measure of the uncertainty can be obtained by using the systematic error in Br_y from Table 1 of 24%, giving an uncertainty of 5.0 pptv. The VSLS contribution is thus (5.0 ± 5.0) pptv. The relatively constant difference between the OSIRIS and Wamsley curves in Figure 17b down to near-tropospheric values of N_2O suggests that 5–7 pptv is either released in the lowermost stratosphere and/or is transported across the tropopause already in inorganic form. The lowest tropical altitude contributing to these results is 18 km (17–19 km layer) which corresponds to an age of air of up to 4–5 months. This places an upper limit of ~4 months on the lifetime of the VSLS candidate species. This would not seem to contradict any current views as, of the VSLS proposed by *WMO* [2007], only CH_2BrCl exceeds this with a lifetime of 5 months with an estimated mixing ratio of only 0.3 pptv in the tropical tropopause layer [*WMO*, 2007]. The single largest contributor is thought to be CH_2Br_2 which has a lifetime of ~4 months and contributes ~1.8 pptv to inorganic bromine (0.9 pptv mixing ratio) [*WMO*, 2007].

7. Summary and Conclusions

[54] A 7+ year (2001–2008) data set of stratospheric BrO profiles measured by the Optical Spectrograph and InfraRed Imager System (OSIRIS) satellite instrument has been presented. Zonal mean radiance spectra were computed for each day and inverted to yield effective daily zonal mean BrO profiles from 16–36 km. Single profile precision was found to be about 30% with an effective resolution of 3–5 km, respectively, throughout much of the retrieval range. The systematic error is estimated to be about 17%. It was necessary to implement a temperature-dependent slit function width to allow for a blurring of the image due to a cooling during eclipse season. Comparisons between individual profiles and monthly means are found to agree to typically 30% with other observations of BrO from ground-based, balloon, and satellite instruments. However, it is noted that OSIRIS displayed a larger seasonal cycle than some of the correlative data.

[55] A BrO climatology was presented, and its abundance, morphology, and correlation with NO_2 were determined to be consistent with the current understanding of bromine chemistry. Monthly mean BrO, in concert with photochemical modeling, were used to derive monthly Br_y maps. Two methods of calculating total stratospheric Br_y, one comparing partial columns of BrO to model simulations, the other involving correlations between Br_y and N_2O, presented a consistent picture and suggest (21.0 ± 5.0) pptv with a VSLS contribution of (5.0 ± 5.0) pptv. The Br_y-N_2O correlation also placed an upper limit of the lifetime of VSLS species of about 4 months. OSIRIS v4.0 BrO data are available for download in day-based HDFEOS-5 format from http://osirus.usask.ca.

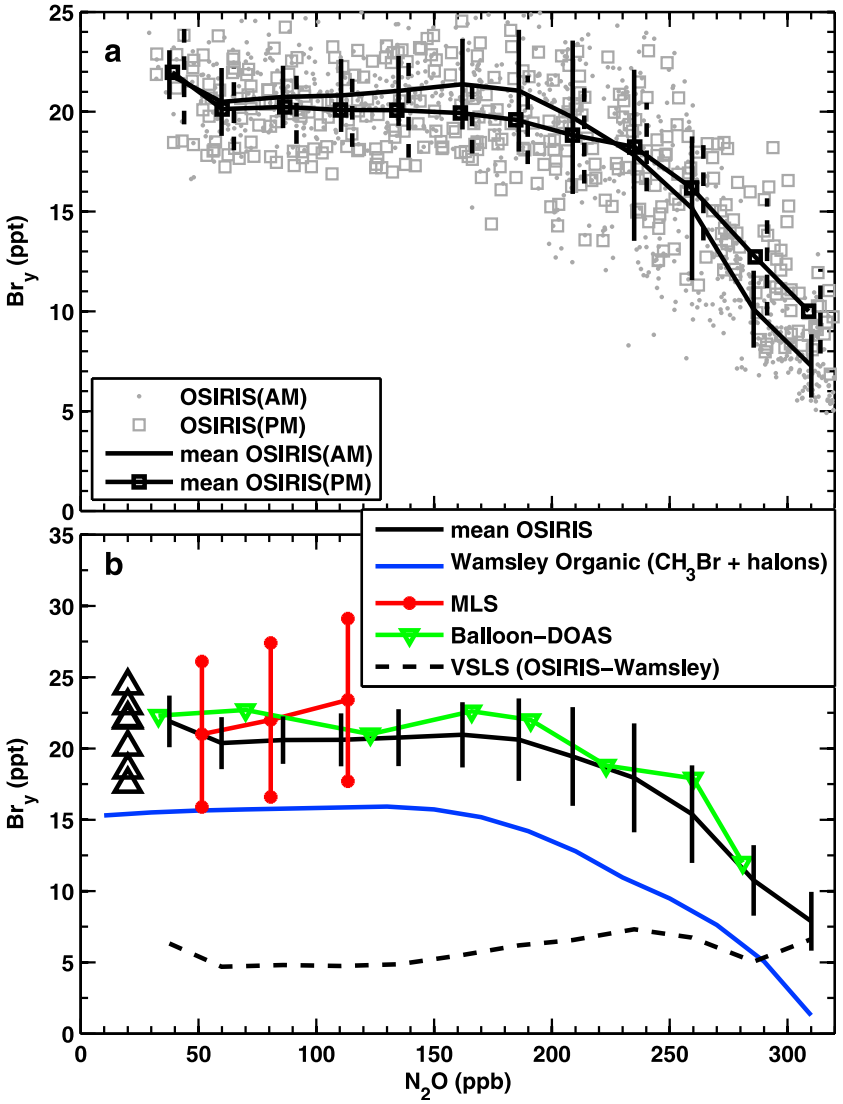

Figure 17. (a) Tracer correlation plot of OSIRIS Br_y and Odin/Submillimetre and Millimetre Radiometer N_2O monthly mean from 40°S to 40°N shown separately for AM and PM measurements. Each symbol represents an individual altitude/latitude. Lines represent mean Br_y averaged over 20 ppbv wide bins in N_2O and their 1σ standard deviation (shown dashed for PM values). (b) Tracer correlation of Br_y and N_2O for different data sources. The open triangles represent inferred total Br_y from other studies (without accompanying N_2O). MLS, Microwave Limb Sounder.

[56] **Acknowledgments.** Odin is a Swedish-led satellite project funded jointly by Sweden (SNSB), Canada (CSA), France (CNES) and Finland (Tekes). Odin is also partially funded as a European Space Agency Third Party Mission. Ground-based UV-visible BrO profiling activities at Harestua and OHP are funded by the PRODEX 9 project SECPEA. The SAOZ flights were carried out by the CNES, ESRANGE and IPMet balloon teams with the support of the EU projects Stratospheric BrO, HIBISCUS, AMMA and SCOUT-O3. Their data are available at http://ether.ipsl.jussieu.fr. C.M. thanks Yves Rochon for helpful discussions. The authors acknowledge three anonymous reviewers for their helpful comments.

References

Aliwell, S. R., et al. (2002), Analysis for BrO in zenith-sky spectra: An intercomparison exercise for analysis improvement, *J. Geophys. Res.*, *107*(D14), 4199, doi:10.1029/2001JD000329.

Bauman, J. J., P. B. Russell, M. A. Geller, and P. Hamill (2003), A stratospheric aerosol climatology from SAGE II and CLAES measurements: 2. Results and comparisons, 1984–1999, *J. Geophys. Res.*, *108*(D13), 4383, doi:10.1029/2002JD002993.

Bogumil, K., et al. (2003), Measurements of molecular absorption spectra with the SCIAMACHY pre-flight model: Instrument characterization and reference data for atmospheric remote-sensing in the 230-2380 nm region, *J. Photochem. Photobiol. A*, *157*(2–3), 167–184, doi:10.1016/S1010-6030(03)00062-5.

Bourassa, A. E., D. A. Degenstein, R. L. Gattinger, and E. J. Llewellyn (2007), Stratospheric aerosol retrieval with optical spectrograph and infrared imaging system limb scatter measurements, *J. Geophys. Res.*, *112*, D10217, doi:10.1029/2006JD008079.

Bovensmann, H., J. P. Burrows, M. Buchwitz, J. Frerick, S. Noël, V. V. Rozanov, K. V. Chance, and A. P. H. Goede (1999), SCIAMACHY: Mission objectives and measurement modes, *J. Atmos. Sci.*, *52*, 127–149.

Brohede, S. M., et al. (2007a), Validation of Odin/OSIRIS stratospheric NO_2 profiles, *J. Geophys. Res.*, *112*, D07310, doi:10.1029/2006JD007586.

Brohede, S., C. A. McLinden, G. Berthet, C. S. Haley, D. Murtagh, and C. E. Sioris (2007b), A stratospheric NO_2 climatology from Odin/OSIRIS limb-scatter measurements, *Can. J. Phys.*, *85*(11), 1253–1274, doi:10.1139/P07-141.

Brohede, S., C. A. McLinden, J. Urban, C. S. Haley, A. I. Jonsson, and D. Murtagh (2008), Odin stratospheric proxy NO_y measurements and climatology, *Atmos. Chem. Phys.*, *8*, 5731–5754.

Brune, W. H., D. W. Toohey, J. G. Anderson, W. L. Starr, J. F. Vedder, and E. F. Danielsen (1988), In situ northern mid-latitude observations of ClO, O3, and BrO in the wintertime lower stratosphere, *Science*, *242*, 558–562.

Chartrand, D. J., and J. C. McConnell (2000), Heterogeneous chemistry and the O_3 budget in the lower mid-latitude stratosphere, *J. Atmos. Chem.*, *35*, 109–149.

Degenstein, D. A., E. J. Llewellyn, and N. D. Lloyd (2003), Volume emission rate tomography from a satellite platform, *Appl. Opt.*, *42*(8), 1441–1450.

Degenstein, D. A., A. E. Bourassa, C. Z. Roth, and E. J. Llewellyn (2009), Limb scatter ozone retrieval from 10 to 60 km using a Multiplicative Algebraic Reconstruction Technique, *Atmos. Chem. Phys.*, *9*, 6521–6529.

Dorf, M., et al. (2006), Balloon-borne stratospheric BrO measurements: Comparison with Envisat/SCIAMACHY BrO limb profiles, *Atmos. Chem. Phys.*, *6*, 2483–2501.

Dorf, M., A. Butz, C. Camy-Peyret, M. P. Chipperfield, L. Kritten, and K. Pfeilsticker (2008), Bromine in the tropical troposphere and stratosphere as derived from balloon-borne BrO observations, *Atmos. Chem. Phys.*, *8*, 7265–7271.

Frisk, U., et al. (2003), The Odin satellite I: Radiometer design and test, *Astron. Astrophys.*, *402*(3), L27–L34, doi:10.1051/0004-6361:20030335.

Gattinger, R. L., D. A. Degenstein, and E. J. Llewellyn (2006), Optical Spectrograph and Infra-Red Imaging System (OSIRIS) observations of mesospheric OH $A^2\Sigma$–$X^2\Pi$ 0–0 and 1–1 band resonance emissions, *J. Geophys. Res.*, *111*, D13303, doi:10.1029/2005JD006369.

Griffioen, E., and L. Oikarinen (2000), LIMBTRAN: A pseudo three-dimensional radiative transfer model for the limb-viewing imager OSIRIS on the Odin satellite, *J. Geophys. Res.*, *105*(D24), 29,717–29,730.

Haley, C. S., and S. Brohede (2007), Status of the Odin/OSIRIS stratospheric O_3 and NO_2 data products, *Can. J. Phys.*, *85*(11), 1177–1194.

Haley, C. S., S. M. Brohede, C. E. Sioris, E. Griffioen, D. P. Murtagh, I. C. McDade, P. Eriksson, E. J. Llewellyn, A. Bazureau, and F. Goutail (2004), Retrieval of stratospheric O_3 and NO_2 profiles from Odin/OSIRIS limb-scattered sunlight measurements, *J. Geophys. Res.*, *109*, D16303, doi:10.1029/2004JD004588.

Hendrick, F., et al. (2007), Retrieval of stratospheric and tropospheric BrO profiles and columns using ground-based zenith-sky DOAS observations at Harestua, 60°N, *Atmos. Chem. Phys.*, *7*, 4869–4885.

Hendrick, F., P. V. Johnston, M. De Mazière, C. Fayt, C. Hermans, K. Kreher, N. Theys, A. Thomas, and M. Van Roozendael (2008), One-decade trend analysis of stratospheric BrO over Harestua (60°N) and Lauder (45°S) reveals a decline, *Geophys. Res. Lett.*, *35*, L14801, doi:10.1029/2008GL034154.

Hendrick, F., et al. (2009), Multi-year comparison of stratospheric BrO vertical profiles retrieved from SCIAMACHY limb and ground-based UV-visible measurements, *Atmos. Meas. Tech.*, *2*, 273–285.

Höpfner, M., J. Orphal, T. von Clarmann, G. Stiller, and H. Fischer (2009), Stratospheric $BrONO_2$ observed by MIPAS, *Atmos. Chem. Phys.*, *9*, 1735–1746.

Johnson, D. G., W. A. Traub, K. V. Chance, and K. W. Jucks (1995), Detection of HBr and upper limit for HOBr: Bromine partitioning in the stratosphere, *Geophys. Res. Lett.*, *22*, 1373–1376.

Kerzenmacher, T., et al. (2008), Validation of NO_2 and NO from the Atmospheric Chemistry Experiment (ACE), *Atmos. Chem. Phys.*, *8*, 5801–5841.

Kovalenko, L. J., et al. (2007), Validation of Aura Microwave Limb Sounder BrO observations in the stratosphere, *J. Geophys. Res.*, *112*, D24S41, doi:10.1029/2007JD008817.

Krecl, P., C. S. Haley, J. Stegman, S. M. Brohede, and G. Berthet (2006), Retrieving the vertical distribution of stratospheric OClO from Odin/OSIRIS limb-scattered sunlight measurements, *Atmos. Chem. Phys.*, *6*, 1879–1894.

Laube, J. C., A. Engel, H. Bnisch, T. Möbius, D. R. Worton, W. T. Sturges, K. Grunow, and U. Schmidt (2008), Contribution of very short-lived organic substances to stratospheric chlorine and bromine in the tropics: A case study, *Atmos. Chem. Phys.*, *8*, 7325–7334.

Llewellyn, E. J., et al. (2004), The OSIRIS instrument on the Odin satellite, *Can. J. Phys.*, *82*(6), 411–422, doi:10.1139/P04-005.

McElroy, M. B., R. J. Salawitch, S. C. Wofsy, and J. A. Logan (1986), Reductions of Antarctic ozone due to synergistic interactions of chlorine and bromine, *Nature*, *321*, 759–762, doi:10.1038/321759a0.

McLinden, C. A., and C. S. Haley (2008), Odin/OSIRIS observations of stratospheric NO_3 through sunrise and sunset, *Atmos. Chem. Phys.*, *8*, 5529–5534.

McLinden, C. A., S. C. Olsen, B. Hannegan, O. Wild, M. J. Prather, and J. Sundet (2000), Stratospheric ozone in 3-D models: A simple chemistry and the cross-tropopause flux, *J. Geophys. Res.*, *105*(D11), 14,653–14,665, doi:10.1029/2000JD900124.

McLinden, C. A., J. C. McConnell, E. Griffioen, and C. T. McElroy (2002a), A vector radiative transfer model for the Odin/OSIRIS project, *Can. J. Phys.*, *80*(4), 375–393, doi:10.1139/p01-156.

McLinden, C. A., J. C. McConnell, K. Strong, I. C. McDade, R. L. Gattinger, R. King, B. Solheim, E. J. Llewellyn, and W. F. J. Evans (2002b), The impact of the OSIRIS grating efficiency on total radiance and trace-gas retrievals, *Can. J. Phys.*, *80*(4), 469–481, doi:10.1139/p01-151.

McLinden, C. A., C. S. Haley, and E. J. Llewellyn (2004), Derivation of polarization from Odin/OSIRIS limb spectra, *Geophys. Res. Lett.*, *31*, L20112, doi:10.1029/2004GL020825.

McLinden, C. A., C. S. Haley, and C. E. Sioris (2006), Diurnal effects in limb scatter observations, *J. Geophys. Res.*, *111*, D14302, doi:10.1029/2005JD006628.

McLinden, C. A., V. E. Fioletov, C. S. Haley, N. Lloyd, C. Roth, D. Degenstein, A. Bourassa, C. T. McElroy, and E. J. Llewellyn (2007), An evaluation of Odin/OSIRIS limb pointing and stratospheric ozone through comparisons with ozonesondes, *Can. J. Phys.*, *85*, 1125–1141.

McPeters, R. D., G. J. Labow, and J. A. Logan (2007), Ozone climatological profiles for satellite retrieval algorithms, *J. Geophys. Res.*, *112*, D05308, doi:10.1029/2005JD006823.

Murtagh, D., et al. (2002), An overview of the Odin atmospheric mission, *Can. J. Phys.*, *80*(4), 309–319.

Nagatani, R. M., and J. E. Rosenfield (1993), Temperature, net heating and circulation, in The Atmospheric Effects of Stratospheric Aircraft: Report of the 1992 Models and Measurements Workshop, *NASA Ref. Publ. 1292*, edited by M. J. Prather and E. E. Remsberg, pp. A1–A47, NASA, Washington, D. C.

Nolt, I. G., et al. (1997), Stratospheric HBr concentration profile obtained from far-infrared emission spectroscopy, *Geophys. Res. Lett.*, *3*, 281–284.

Olsen, S. C., C. A. McLinden, and M. J. Prather (2001), Stratospheric N_2O–NO_y system: Testing uncertainties in a three-dimensional framework, *J. Geophys. Res.*, *106*(D22), 28,771–28,784.

Pfeilsticker, K., W. Sturges, H. Bösch, C. Camy-Peyret, M. Chipperfield, A. Engel, R. Fitzenberger, M. Müller, S. Payan, and B.-M. Sinnhuber (2000), Lower stratospheric organic and inorganic bromine budget for the artic winter 1998/99, *Geophys. Res. Lett.*, *27*, 3305–3308.

Prather, M. (1992), Catastrophic loss of stratospheric ozone in dense volcanic clouds, *J. Geophys. Res.*, *97*(D9), 10,187–10,191, doi:10.1029/92JD00845.

Pundt, I., J.-P. Pommereau, M. P. Chipperfield, M. Van Roozendael, and F. Goutail (2002), Climatology of the stratospheric BrO vertical distribution by balloon-borne UV-visible spectrometry, *J. Geophys. Res.*, *107*(D24), 4806, doi:10.1029/2002JD002230.

Richter, A., F. Wittrock, M. Eisinger, and J. P. Burrows (1998), GOME observations of tropospheric BrO in northern hemispheric spring and summer 1997, *Geophys. Res. Lett.*, 2683–2686.

Rodgers, C. D. (2000), *Inverse Methods for Atmospheric Sounding: Theory and Practice*, 1st ed., World Sci., River Edge, N. J.

Salawitch, R. J., C. E. Sioris, D. K. Weisenstein, P. O. Wennberg, L. J. Kovalenko, K. Chance, M. K. W. Ko, and C. A. McLinden (2005), Sensitivity of ozone to bromine in the lower stratosphere, *Geophys. Res. Lett.*, *32*, L05811, doi:10.1029/2004GL021504.

Sander, S. P., et al. (2006), JPL 2006: Chemical kinetics and photochemical data for use in atmospheric studies: Evaluation 15, *JPL Publ. 062*, Jet Propul. Lab., Pasadena, Calif.

Sinnhuber, B.-M., et al. (2005), Global observations of stratospheric bromine monoxide from SCIAMACHY, *Geophys. Res. Lett.*, *32*, L20810, doi:10.1029/2005GL023839.

Sioris, C. E., W. F. J. Evans, R. L. Gattinger, I. C. McDade, D. Degenstein, and E. J. Llewellyn (2002), Ground-based Ring effect measurements with the OSIRIS DM, *Can. J. Phys.*, *80*, 483–491.

Sioris, C. E., et al. (2003), Stratospheric profiles of nitrogen dioxide observed by Optical Spectrograph and Infrared Imager System on the Odin satellite, *J. Geophys. Res.*, *108*(D7), 4215, doi:10.1029/2002JD002672.

Sioris, C. E., et al. (2006), Latitudinal and vertical distribution of bromine monoxide in the lower stratosphere from SCIAMACHY limb scattering measurements, *J. Geophys. Res.*, *111*, D14301, doi:10.1029/2005JD006479.

Solomon, S., R. W. Sanders, M. A. Carroll, and A. L. Schmeltekopf (1989), Visible and near-ultraviolet spectroscopy at McMurdo Station, Antarctica: 5. Observations of the diurnal variations of BrO and OClO, *J. Geophys. Res.*, *94*(D9), 11,393–11,403.

Spencer, J. E., and F. S. Rowland, (1978), Bromine nitrate and its stratospheric significance, *J. Phys. Chem.*, *82*, 7–10.

Urban, J., et al. (2005), Odin/SMR limb observations of stratospheric trace gases: Level 2 processing of ClO, N_2O, HNO_3, and O_3, *J. Geophys. Res.*, *110*, D14307, doi:10.1029/2004JD005741.

Vandaele, A. C., C. Hermans, P. C. Simon, M. Carleer, R. Colin, S. Fally, M. F. Mérienne, A. Jenouvrier, and B. Coquart (1998), Measurements of the NO_2 absorption cross-section from 42,000 cm^{-1} to 10,000 cm^{-1} (238–1000 nm) at 220 K and 294 K, *J. Quant. Spectrosc. Radiat. Transfer*, *59*(3–5), 171–184, doi:10.1016/S0022-4073(97)00168-4.

von Savigny, C., et al. (2003), Stratospheric ozone profiles retrieved from limb scattered sunlight radiance spectra measured by the OSIRIS instrument on the Odin satellite, *Geophys. Res. Lett.*, *30*(14), 1755, doi:10.1029/2002GL016401.

Wamsley, P. R., et al. (1998), Distribution of halon-1211 in the upper troposphere and lower stratosphere and the 1994 total bromine budget, *J. Geophys. Res.*, *103*(D1), 1513–1526, doi:10.1029/97JD02466.

Wilmouth, D. M., T. F. Hanisco, N. M. Donahue, and J. G. Anderson (1999), Fourier transform ultraviolet spectroscopy of the $A(^2\Pi_{3/2}) \leftarrow X(^2\Pi_{3/2})$ transition of BrO, *J. Phys. Chem. A*, *103*, 8935–8945.

World Meteorological Organization (WMO) (2007), Scientific assessment of ozone depletion: 2006, Global *Ozone Res. and Monit. Proj., Rep. 50*, Geneva.

J. P. Burrows, W. Lotz, A. Rozanov, and B.-M. Sinnhuber, Institute of Environmental Physics, University of Bremen, PO Box 330440, D-28334 Bremen, Germany.

D. A. Degenstein, E. J. Llewellyn, and N. D. Lloyd, Institute of Space and Atmospheric Studies, University of Saskatchewan, 116 Science Pl., Saskatoon, Saskatchewan S7N 5E2, Canada.

F. Goutail and J. P. Pommereau, Service d'Aéronomie, CNRS, Reduit de Verrières–BP3, F-91371 Verrières-le-Buisson, France.

C. S. Haley, Centre for Research in Earth and Space Science, York University, 4700 Keele St., Toronto, ON M3J 1P3, Canada.

F. Hendrick and M. Van Roozendael, BIRA-IASB, Ave. Circulaire 3, B-1180 Brussels, Belgium.

C. A. McLinden and C. E. Sioris, Air Quality Research Division, Environment Canada, 4905 Dufferin St., Toronto, ON M3H 5T4, Canada. (chris.mclinden@ec.gc.ca)